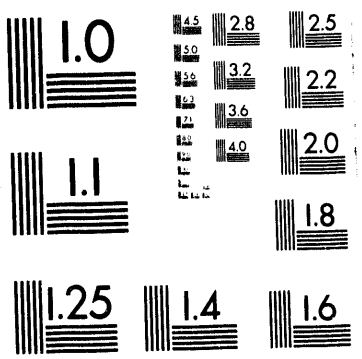
1.0
1.1
1.25
1.4
1.6
1.8
2.0
2.2
2.5
2.8
3.2
3.6
4.0
4.5
5.0
5.6

1 of 1

ANL/MCT/PP--74905

Estimation of Mechanical Properties of Cast Stainless Steels during Thermal Aging in LWR Systems*

O. K. Chopra

Materials and Components Technology Division
Argonne National Laboratory
9700 South Cass Avenue
Argonne, Illinois 60439 USA

October 1991

* Work supported by the Office of Nuclear Regulatory Research, U.S. Nuclear Regulatory Commission, FIN No. A2243, Project Manager: J. Muscara.

ESTIMATION OF MECHANICAL PROPERTIES OF CAST STAINLESS STEELS DURING THERMAL AGING IN LWR SYSTEMS*

O. K. CHOPRA
Materials and Components Technology Division, Argonne National Laboratory
9700 South Cass Avenue, Argonne, Illinois 60439

A procedure and correlations are presented for predicting Charpy-impact energy, tensile flow stress, fracture toughness J-R curve, and J_{IC} of aged cast stainless steels from known material information. The "saturation" impact strength and fracture toughness of a specific cast stainless steel, i.e., the minimum value that would be achieved for the material after long-term service, is estimated from the chemical composition of the steel. Mechanical properties as a function of time and temperature of reactor service are estimated from impact energy and flow stress of the unaged material and the kinetics of embrittlement, which are also determined from chemical composition. The J_{IC} values are determined from the estimated J-R curve and flow stress. Examples of estimating mechanical properties of cast stainless steel components during reactor service are presented. A common "predicted lower-bound" J-R curve for cast stainless steels of unknown chemical composition is also defined for a given grade of steel, ferrite content, and temperature.

1 Introduction

Investigations at Argonne National Laboratory (ANL) [1–4] and elsewhere [5–12] have shown that thermal embrittlement of cast stainless steels used for components of light water reactors (LWRs), e.g., valve bodies, pump casings, and primary coolant piping, can occur during the reactor design lifetime of 40 y. Thermal aging of cast stainless steels at reactor operating temperatures, i.e., 280–320°C (536–608°F) increases hardness and tensile strength and decreases ductility, impact strength, and fracture toughness of the material. The Charpy transition curve shifts to higher temperatures. Most studies on thermal embrittlement of cast stainless steels involve simulation of end-of-life reactor conditions by accelerated aging at higher temperatures, viz., 400°C (752°F), because the time period for operation of power plants (≈40 y) is far longer than can generally be considered for laboratory studies. Thus, estimates of the loss of fracture toughness of cast stainless steel components are based on an Arrhenius extrapolation of high-temperature data to reactor operating conditions.

A procedure and correlations are presented for predicting mechanical properties of cast stainless steel components during thermal aging in LWRs at 280–330°C (536–626°F). These correlations are updates of those presented earlier [13,14]. The present analysis focused on developing correlations for fracture properties in terms of material information in certified material test records (CMTRs) and on ensuring that the correlations are adequately conservative for cast stainless steels defined by ASTM Specification A 351. These correlations do not consider the effect of microstructural differences that may arise from

* Work supported by the Office of Nuclear Regulatory Research, U.S. Nuclear Regulatory Commission, FIN No. A2243, Project Manager: J. Muscara.

Mechanical properties of a specific cast stainless steel are estimated from the extent and kinetics of thermal embrittlement. The extent of thermal embrittlement is characterized by room-temperature (RT) "normalized" Charpy-impact energy (Charpy-impact energy per unit fracture area). A correlation for the extent of embrittlement at "saturation," i.e., the minimum impact energy that can be achieved for the material after long-term aging, is given in terms of chemical composition. The results indicate that Charpy-impact energy can be <85 J/cm^2 (<50 ft·lb) for cast stainless steels with ferrite contents as low as 10%.

Extent of thermal embrittlement as a function of time and temperature of reactor service is estimated from the extent of embrittlement at saturation and from the correlations describing the kinetics of embrittlement, which are also given in terms of the chemical composition of the steel. The fracture toughness J-R curve for the material is then obtained from the correlation between fracture toughness parameters and the RT Charpy-impact energy used to characterize the extent of thermal embrittlement. A common lower-bound J-R curve for cast stainless steels of unknown chemical composition is also defined for a given material grade and temperature. In addition, correlations are presented for estimating the increase in tensile flow stress from data on the kinetics of thermal embrittlement; initial tensile flow stress of the unaged material is needed to determine the flow stress of the aged material. Fracture toughness parameters, e.g., J_{IC} and tearing modulus, are determined from the estimated J-R curve and tensile flow stress. Examples of estimating mechanical properties of cast stainless steel components during reactor service are included.

2 Mechanism of Thermal Embrittlement

Thermal embrittlement of cast duplex stainless steels results in brittle fracture associated with either cleavage of the ferrite or separation of the ferrite/austenite phase boundary. The degree of thermal embrittlement is controlled by the amount of brittle fracture. Cast stainless steels with poor impact strength exhibit >80% brittle fracture. In some cast steels, a fraction of the material may fail in brittle fashion but the surrounding austenite provides ductility and toughness. Such steels have adequate impact strength even after long-term aging. A predominantly brittle failure occurs when either the ferrite phase is continuous, e.g., in cast material with a large ferrite content, or the ferrite/austenite phase boundary provides an easy path for crack propagation, e.g., in high-C grades of cast steels that contain phase-boundary carbides. Consequently, the amount, size, and distribution of ferrite in the duplex structure and phase-boundary carbides are important parameters that control the extent of thermal embrittlement. The extent of thermal embrittlement increases with increased ferrite content. The low-C CF-3 steels are the most resistant, and the Mo-bearing, high-C CF-8M steels are the least resistant to thermal embrittlement.

Thermal aging of cast stainless steels at <500°C (<932°F) leads to precipitation of additional phases in the ferrite, e.g., formation of a Cr-rich α' phase by spinodal decomposition; nucleation and growth of α'; precipitation of a Ni- and Si-rich G phase, $M_{23}C_6$, and γ_2 (austenite); and additional precipitation and/or growth of existing carbides at the ferrite/austenite phase boundaries [15-21]. Formation of α' phase is the primary strengthening mechanism for ferrite, which increases strain-hardening and local tensile

stress. Consequently, the critical stress level for brittle fracture is achieved at higher temperatures. Other precipitate phases in ferrite have little or no effect on the extent of thermal embrittlement.

Phase-boundary separation generally occurs in the high-C steels because of the presence of large $M_{23}C_6$ carbides at the phase boundaries. For CF-8 steels, the phase-boundary carbides form during production heat treatment of the casting. Consequently, unaged CF-8 steels exhibit low lower-shelf energy and high mid-shelf Charpy transition temperature (CTT) relative to the CF-3 steels. The fracture mode for CF-8 steels in the lower-shelf or transition-temperature regime is predominantly phase-boundary separation [2-4]. In contrast, CF-3 steels show dimpled ductile failure. Fracture by phase-boundary separation is observed in only a few heats of unaged CF-8M steels and is dependent on whether the material contains phase-boundary carbides. Materials aged at 450°C (842°F) show significant precipitation of phase-boundary carbides (also nitrides in high-N steels) and a large decrease in ferrite content of the material [3,4]. At reactor temperatures, such processes either do not occur or their kinetics are extremely slow. Consequently, data obtained at 450°C aging do not reflect the mechanisms active under reactor operating conditions, and extrapolation of the 450°C data to predict the extent of thermal embrittlement at reactor temperatures is not valid.

The kinetics of thermal embrittlement of cast stainless steels are controlled primarily by the kinetics of ferrite strengthening, i.e., the size and spacing of Cr fluctuations produced by spinodal decomposition of ferrite. Small changes in the constituent elements of the material can cause the kinetics of thermal embrittlement to vary significantly. Activation energies of thermal embrittlement can range from 65 to 230 kJ/mole (15 to 55 kcal/mole). Also, the aging behavior at 400°C (752°F) shows significant heat-to-heat variation. The decrease in Charpy-impact energy during thermal aging at 400°C for various heats of cast stainless steels used in studies at ANL [3,4], Georg Fischer Co. (GF) [5], Framatome (FRA) [10],and Electric Power Research Institute (EPRI) [12] is shown in Fig. 1. The results indicate that all materials reach a saturation impact energy, i.e., minimum value that would be achieved by the material after long-term aging. Saturation impact energy, in general, decreases with an increase in ferrite content or the concentration of C and N in the steel. As discussed above, both of these factors promote brittle fracture.

Figure 1 also indicates that the time for aging at 400°C (752°F) for a given decrease in impact energy varies more than 2 orders of magnitude for the various heats. Production heat treatment, and possibly the casting process, influence aging behavior at 400°C and, therefore, the kinetics of thermal embrittlement. The log of the aging time at 400°C for a 50% reduction in Charpy-impact energy has been shown to be a useful parameter for characterizing the kinetics of thermal embrittlement [13]. Activation energy for thermal embrittlement is high for steels that show fast embrittlement at 400°C, and low for those that show slow embrittlement at 400°C. Also, cast materials with high activation energy of embrittlement do not contain G phase and those with low activation energy contain G phase. It is likely that material parameters, e.g., production heat treatment, that influence the kinetics of thermal embrittlement also affect G-phase precipitation; the physical presence of G phase has little or no effect on either the extent or kinetics of embrittlement.

3 Extent of Embrittlement

Charpy-impact data obtained at RT indicate that, for a specific heat of cast stainless steel, a saturation value of minimum impact energy is reached after long-term aging. The saturation impact energy decreases with an increase in the amount of brittle fracture, i.e., in materials with large ferrite content, which provides a path for brittle fracture. An increase in the concentration of C or N in the steel also increases the extent of thermal embrittlement because of the contribution to phase-boundary carbides or nitrides and the subsequent fracture by phase-boundary separation. Furthermore, Charpy-impact data for several heats of cast stainless steel indicate that impact energy decreases with an increase in Cr content, irrespective of the ferrite content of the steel [20]. The concentration of Ni and Si in the steel, i.e., the elements that promote G-phase formation, also appear to increase the extent of thermal embrittlement of Mo-bearing CF-8M steels.

The variation of this saturation impact energy C_{Vsat} for different materials can be expressed in terms of a material parameter Φ that is determined from the chemical composition and ferrite content of the materials. The ferrite content is calculated in terms of the Hull's equivalent factors [22]

$$Cr_{eq} = Cr + 1.21(Mo) + 0.48(Si) - 4.99 \quad (1)$$

and

$$Ni_{eq} = (Ni) + 0.11(Mn) - 0.0086(Mn)^2 + 18.4(N) + 24.5(C) + 2.77, \quad (2)$$

where chemical composition is in wt.%. The concentration of N is often not available in the CMTR; if not known, it is assumed to be 0.04 wt.%. The ferrite content δ_c is given by

$$\delta_c = 100.3(Cr_{eq}/Ni_{eq})^2 - 170.72(Cr_{eq}/Ni_{eq}) + 74.22. \quad (3)$$

Different correlations are used to estimate the saturation impact energy of the various grades of cast stainless steel. For CF-3 and CF-8 steels, the material parameter Φ is expressed as

$$\Phi = \delta_c(Cr + Si)(C + 0.4N), \quad (4)$$

and the saturation value of RT impact energy C_{Vsat} is given by

$$\log_{10}C_{Vsat} = 1.15 + 1.36\exp(-0.035\Phi). \quad (5)$$

For the Mo-bearing CF-8M steels, the material parameter Φ is expressed as

$$\Phi = \delta_c(Ni + Si + Mn)^2(C + 0.4N)/5. \quad (6)$$

The saturation value of RT impact energy C_{Vsat} for steels with < 10% Ni is given by

$$\log_{10}C_{Vsat} = 1.10 + 2.12\exp(-0.041\Phi), \quad (7)$$

and for steels with >10% Ni by

$$\log_{10}C_{Vsat} = 1.10 + 2.64\exp(-0.064\Phi). \quad (8)$$

$$\log_{10}C_{Vsat} = 1.10 + 2.64\exp(-0.064\Phi). \quad (8)$$

The N content in Eqs. 4 and 6 can be assumed to be 0.04 wt.% if the value is not known. The RT saturation impact energy can also be estimated directly from the chemical composition of the steel without the introduction of the ϕ parameter. For CF-3 and CF-8 steels, C_{Vsat} (J/cm^2) is given by

$$\log_{10}C_{Vsat} = 5.64 - 0.006\delta_c - 0.185Cr + 0.273Mo - 0.204Si + 0.044Ni - 2.12(C + 0.4N), \quad (9)$$

and for CF-8M steels by

$$\log_{10}C_{Vsat} = 7.28 - 0.011\delta_c - 0.185Cr - 0.369Mo - 0.451Si - 0.007Ni - 4.71(C + 0.4N). \quad (10)$$

The saturation impact energy for a specific cast stainless steel should be determined using both the methods given in Eqs. 4–10, and the lower value is then used for estimating mechanical properties.

The saturation values of RT impact energy for CF-3 and CF-8 steels predicted by Eqs. 4 and 5 and those observed experimentally at ANL [3,4], GF [5], FRA [10], EPRI [12], Electricité de France (EdF) [7], and Central Electricity Generation Board (CEGB) [8,9] are shown in Fig. 2a. The chemical composition, ferrite content, and saturation RT Charpy-impact energy of the materials from ANL, GF, FRA, Westinghouse (WH), and EPRI are given in Table 1. The difference between the predicted and observed values is $\leq \pm 15\%$ for most of the materials. The observed RT impact energy at saturation and the values predicted by Eqs. 6–8 for CF-8M steels are shown in Figs. 2b and 2c for the data from ANL [3,4], GF [5], WH [6], (EdF) [7] and FRA [10] studies. The difference between observed and predicted values for the CF-8M steel is larger than that for the CF-3 or CF-8 steels. The correlations expressed in Eqs. 4–10 do not include Nb, and may not be conservative for Nb-bearing steels.

4 Kinetics of Embrittlement

Room-temperature impact energy as a function of time and temperature of aging is estimated from the RT saturation impact energy C_{Vsat} (J/cm^2) and the kinetics of embrittlement. The decrease in RT Charpy-impact energy C_V (J/cm^2) with time is expressed as

$$\log_{10}C_V = \log_{10}C_{Vsat} + \beta\{1 - \tanh[(P - \theta)/\alpha]\}, \quad (11)$$

where β is half the maximum change in $\log C_V$, θ is the log of the time at 400°C (752°F) to achieve 50% reduction in impact energy, and α is a shape factor. The aging parameter P is the log of the aging time for a specific degree of embrittlement and is defined by

$$P = \log_{10}[t] - \frac{1000Q}{19.143}\left[\frac{1}{T_s+273} - \frac{1}{673}\right], \quad (12)$$

where Q is the activation energy (kJ/mole) and t and T_s are the time (h) and temperature (°C) of aging. Equation 12 assumes aging at 400°C as the baseline aging behavior for the material and parameter P is the log of the aging time at 400°C. The data obtained at 450°C

excluded from the analysis. The values of the constants in Eqs. 10 and 11 for the various materials are given in Table 1. The constant β is defined in terms of the initial impact energy of the unaged material $C_{V_{int}}$ and the saturation impact energy $C_{V_{sat}}$, thus

$$\beta = (\log_{10}C_{V_{int}} - \log_{10}C_{V_{sat}})/2. \quad (13)$$

Examination of the data for the kinetics of thermal embrittlement suggests that the shape factor α increases linearly with $\log_{10}C_{V_{sat}}$. A best fit of the data for the various heats yields the expression

$$\alpha = -0.585 + 0.795\log_{10}C_{V_{sat}}. \quad (14)$$

$C_{V_{sat}}$ can be calculated from correlations presented in Section 3 if the chemical composition is known. In practice, the initial impact energy is unlikely to be available. Mechanical-property data indicate that Charpy-impact energy of cast stainless steels is typically 200 ±20 J/cm^2, however, it can be as low as 60 J/cm^2 for some steels [4,14].

Activation energy for thermal embrittlement has been expressed in terms of the chemical composition of the cast material. The initial correlations proposed by FRA [10] and ANL [3,4] were either based on very limited data or failed to accurately predict the results from various investigations. A general correlation that is applicable for all chemical compositions within ASTM Specification A 351 and valid for the temperature range 280–400°C (536–752°F) has recently been proposed [13,14]. Activation energy for thermal embrittlement is expressed in terms of both chemical composition and the constant θ, which appears to account for the effects of heat treatment and the casting process on the kinetics of thermal embrittlement. The activation energy Q (kJ/mole) is given by

$$Q = 10\,[74.06 - (7.66 - 0.46\,I_1)\,\theta - 4.35\,Si + 1.38\,I_2\,Mo - 1.67\,Cr - (2.22 + 3.56\,I_1)\,Mn + (108.8 - 75.3\,I_1)\,N], \quad (15)$$

where the indicators $I_1 = 0$ and $I_2 = 1$ for CF-3 or CF-8 steels and assume the values of 1 and 0, respectively, for CF-8M steels. The ANL data, included in the analysis for obtaining Eq. 15, were based on heats that were aged up to 30,000 h at 290–400°C (554–752°F). Also, the data at 290°C were excluded from the analysis for some of the heats. Equation 15 has been optimized using recent ANL data on materials that were aged up to 58,000 h at 290–400°C. The activation energies and values of the constants in Eq. 11 are given in Table 1. The best fit of the data from ANL, FRA, GF, EdF, and CEGB studies (47 heats) yields the expression

$$Q = 10\,[74.52 - 7.20\,\theta - 3.46\,Si - 1.78\,Cr - 4.35\,I_1\,Mn + (148 - 125\,I_1)\,N - 147\,I_2\,C], \quad (16)$$

where the indicators have the same meaning as in Eq. 15. The contribution of Mo and Mn to the kinetics of CF-3 and CF-8 steel is very small; therefore, it is excluded from Eq. 16. For CF-3 and CF-8 steels, the effect of C is included in the new expression.

The estimated and observed values of Q for the ANL, FRA, CEGB, and GF heats are plotted in Fig. 3. The predicted values are within the 95% confidence limits for all the heats. Equation 16 is applicable for compositions within ASTM Specification A 351, with an upper limit of 1.2 wt.% for Mn content. Actual Mn content is used up to 1.2 wt.% and is

assumed to be 1.2 wt.% for steels containing >1.2 wt.% Mn. Furthermore, the values of Q predicted from Eq. 16 should be between 65 kJ/mole minimum and 250 kJ/mole maximum; Q is assumed to be 65 kJ/mole if the predicted values are lower and 250 kJ/mole if the predicted values are higher.

5 Estimation of Impact Energy

The RT Charpy impact energy of a specific cast stainless steel can be estimated from the correlations in Sections 3 and 4. Impact energy at saturation $C_{V_{sat}}$ is determined from the chemical composition of the cast material. Estimation of the decrease in impact energy as a function of time and temperature of service requires additional information, namely, the initial impact energy of the unaged material and the aging behavior at 400°C (752°F), i.e., the value of the constant θ. However, parametric studies indicate that at 280–330°C (536–626°F) the aging response is relatively insensitive to the value of θ. Varying θ between 2.1 and 3.6 results in almost identical aging behavior at 300°C (572°F) and differences in aging behavior at 280–330°C are minimal. A median value of 2.9 for θ can be used in Eqs. 7 and 9 to estimate impact energy of cast stainless steel components in service at 280–330°C.

The RT Charpy-impact energy observed experimentally and that estimated from the chemical composition and initial impact energy of some of the ANL, FRA, and GF heats aged at temperatures between 290–350°C (554–662°F), are shown in Figs. 4 and 5. Estimated values for each heat were calculated as follows. The impact energy at saturation was determined from Eqs. 1–10. The activation energy for embrittlement was obtained from Eq. 16; a θ value of 2.9 was used for all the heats. Then the change in impact energy with time and temperature of service was estimated from Eqs. 11–14. The estimated change in impact energy at temperatures ≤330°C (626°F) is either accurate or slightly conservative for most of the heats. As discussed above, a value of θ can be used to estimate thermal embrittlement at service temperatures of 280–330°C (536–626°F). With an assumed value of 2.9 for θ, estimations of impact energies before saturation will be non-conservative at service temperatures >330°C for heats with $\theta < 2.9$ and at temperatures <280°C for heats with $\theta > 2.9$. A value of 2.5 should be used for estimations at temperatures between 330 and 360°C (626 and 680°F) and a value of 3.3 should be used for estimations at temperatures <280°C (<536°F). Even at 350°C, the estimated impact energies (Figs. 4 and 5) show good agreement with the experimental results because the θ values for the heats shown in the figures are either greater or only slightly lower than 2.9.

6 Tensile Properties

Thermal aging leads to an increase in yield and ultimate stress and a slight decrease in ductility. For all heats, the increase in ultimate stress is substantially greater than the increase in yield stress. Some heats show no change in yield stress. Furthermore, specimens aged for short times at high temperatures, e.g., ≈3,000 h at 400 or 450°C (752 or 842°F), often show a decrease in yield and ultimate stresses.

The tensile data generally agree with the Charpy-impact data, i.e., for a specific heat, the increase in tensile stress corresponds to a decrease in impact energy. The ratio of the tensile flow stress of aged and unaged cast stainless steels at RT and 290°C (554°F) is plotted as a function of a normalized aging parameter in Figs. 6 and 7, respectively. Flow

stress is characterized as the mean of the 0.2% yield and ultimate stresses, and the aging parameter is normalized with respect to a θ value of 2.9. At both temperatures, the increase in flow stress of CF-3 steels is the lowest and that of CF-8M steels the largest. The flow stress ratio $R = (\sigma f_{aged}/\sigma f_{unaged})$ is given by

$$R = a_1 + b_1(P - \theta + 2.9). \quad (17)$$

Equation 17 is valid for ferrite contents >7% and R values between 1 and a constant c_1. Values of the constants a_1, b_1, and c_1 for different grades of steel and test temperatures are given in Table 2.

Experimental and estimated tensile flow stress at 290°C (554°F) and at RT for various heats of aged cast stainless steel are shown in Fig. 8. For each heat, the aging parameter was obtained from Eqs. 12 and 16; because most of the data are for aging temperatures ≥350°C, the actual experimental value of θ was used for all the heats. Tensile flow stress was then estimated from Eq. 17 and the initial flow stress of the materials. The estimated values are within 15% of the observed value for most material and aging conditions.

7 Fracture Toughness

Estimation of J-R Curves

Thermal aging decreases the fracture toughness of cast stainless steels at RT as well as at reactor temperatures, i.e., 280-320°C (536-608°F). The fracture toughness results are consistent with the Charpy-impact data, i.e., unaged and aged materials that show low impact strength also exhibit lower fracture toughness. The fracture toughness J-R curve for a specific cast stainless steel can be estimated from its RT impact energy.

The J-R curve is expressed by the power-law relation $J_d = C\Delta a^n$, where J_d is deformation J (kJ/m^2) per ASTM Specifications E 813-85 and E 1152-87, Δa is crack extension (mm), and C and n, respectively, are the coefficient and exponent of the power-law J-R curve. The coefficient C at room and reactor temperatures and the RT Charpy-impact energy for aged and unaged cast stainless steels are plotted in Fig. 9. Fracture toughness data from ANL, FRA,[10,11] EPRI,[12] Materials Engineering Associates, Inc., (MEA),[23] and The Welding Institute (TWI),[24] studies are included in the figure. At both temperatures, the coefficient C decreaseed with a decrease in impact energy. Separate correlations were obtained for CF-3 or CF-8 steels and for CF-8M steels; the latter showed a larger decrease in fracture toughness for a given impact energy. The correlations used to estimate J-R curves for static-cast materials were obtained by subtracting the value of σ (standard deviation for the fit to the data) from the best-fit curve. They are shown as dash lines in Fig. 9, and help ensure that the estimated J-R curve is conservative for all material and aging conditions. Best-fit correlations were used for centrifugally cast materials. The saturation fracture toughness J-R curve at RT for static-cast CF-3 and CF-8 steels is given by

$$J_d = 49[C_V]^{0.52}[\Delta a]^n, \quad (18)$$

and for static-cast CF-8M steels by

$$J_d = 16[C_V]^{0.67}[\Delta a]^n. \quad (19)$$

At 290–320°C (554–608°F), the J-R curve for static cast CF-8 steels is given by

$$J_d = 102[C_V]^{0.28}[\Delta a]^n, \quad (20)$$

and for static-cast CF-8M steels by

$$J_d = 49[C_V]^{0.41}[\Delta a]^n. \quad (21)$$

For centrifugally cast steels, the constants in Eqs. 18–21 are 57, 20, 134, and 57, respectively. At RT, the exponent n for static- or centrifugally cast steels is given by

$$n = a_2 + b_2 \log_{10} C_V, \quad (22)$$

where the values of the constants a_2 and b_2 for different grades of steel and test temperature are given in Table 3. J-R curve at any intermediate temperature can be linearly interpolated from the estimated values of C and n at RT and at 290°C (554°F).

The fracture toughness J-R curve at saturation for a specific cast stainless steel can be obtained from its chemical composition by using the correlations for $C_{V_{sat}}$ given in Eqs. 1–10 and then using the estimated $C_{V_{sat}}$ in Eqs. 18–22 to obtain the J-R curve. Comparisons of the experimental and estimated J-R curves at saturation, i.e., the minimum fracture toughness that would be achieved for the material by thermal aging, are shown in Figs. 10 – 12. For most heats, the saturation fracture toughness is achieved after aging for ≥5,000 h at 400°C (752°F). The experimental and estimated J-R curves for the unaged materials are also shown for comparison; the J-R curves were estimated from Eqs. 18–22 by using the measured initial RT impact energy $C_{V_{int}}$. The estimated J-R curves show good agreement with the experimental results in most cases and are essentially conservative. The largest difference between the estimated and experimental J-R curves is for centrifugally cast Heats P2 and 205 at RT and for centrifugally cast Heat P2 and static-cast EPRI heat at 290°C; the estimated curves of these heats are 30–50% lower than those obtained experimentally. The experimental J-R curves for Heat 75 aged for 30,000 h at 350°C are lower than those for 10,000-h aging at 400°C (shown in Fig. 11) and are in good agreement with the estimated saturation J-R curve.

Room temperature J-R curves for unaged static-cast Heats 68, 69, and 75 are non-conservative. It is believed that the poor fracture toughness of these unaged static-cast slabs is due to residual stresses introduced in the material during the casting process or production heat treatment. Annealing these heats for a short time at temperatures between 290 and 400°C (554 and 752°F) increased the fracture toughness and decreased the tensile stress without significantly affecting their impact energy [4]. Consequently, the fracture toughness of these heats would initially increase during reactor service before it would decrease due to thermal aging.

The estimated J-R curve after 32 effective full-power years (efpy) of service at 320°C (608°F) is also shown in Figs. 10–12. The results indicate that at 320°C service, fracture toughness of these materials will reach the saturation value or will be close to saturation within the 40-y design life.

The fracture toughness J–R curve for a specific material and aging condition can be obtained by estimating the RT impact energy from the procedure described in Section 5, and then using that value of C_V in Eqs. 18–22 to estimate the J–R curve. Examples of the experimental and estimated J–R curves for several partially aged (i.e., 30,000 h at 320°C) cast stainless steels are shown in Figs. 13 and 14. The estimated J–R curves show good agreement with experimental results.

The fracture–toughness data for unaged cast stainless steels indicate that the J–R curve for some heats are lower than those for wrought stainless steels. The available J–R curve data at 290–320°C (555–610°F) for unaged cast stainless steels are shown in Fig. 15a. The static–cast pump casing ring (Heat C1 with δ_c = 8%) shows the lowest and centrifugally cast pipes (Heat P2 with δ_c = 12% and Heat C1488 with δ_c = 21%) have the highest fracture toughness. Fracture toughness J–R curves for wrought stainless steels are higher than the J–R curve for static–cast pump casing ring; see Fig. 15b. The fracture toughness of unaged cast stainless steels is slightly higher at RT than at 290–320°C (554–608°F). At temperatures up to 320°C, a lower–bound J–R curve for unaged static–cast stainless steels can be expressed as

$$J_d = 400[\Delta a]^{0.40} \tag{23}$$

and for centrifugally cast stainless steels as

$$J_d = 650[\Delta a]^{0.43}. \tag{24}$$

The present correlations account for the degradation of toughness due to thermal aging. They do not explicitly consider the initial fracture properties of the original unaged material. To take this into account, when no information is available on the fracture toughness of the unaged material, the lower–bound estimate given by Eq. 23 or 24 is used as upper bound for the predicted fracture toughness of the aged material, i.e., Eq. 23 or 24 is used when fracture toughness predicted by Eqs. 18–22 is higher than that given by Eq. 23 or 24. If the actual fracture toughness of the unaged material or the initial RT Charpy–impact energy for estimating fracture toughness is known, the use of the higher value may be justified.

The fracture toughness J_{IC} values for aged cast stainless steels can be determined from the estimated J–R curve and flow stress. The experimental and estimated J_{IC} for the various heats aged at ≤350°C are shown in Fig. 16. The chemical composition and the initial Charpy–impact energy and flow stress of the unaged material were used for the estimations. The estimated J_{IC} values show good agreement with the experimental results; for most cases the estimated J_{IC} is lower but within 30% of the observed value.

Lower–bound J–R Curves

For cast stainless steels of unknown chemical composition, lower–bound fracture toughness is defined for a given material grade and temperature. Figure 2 indicates that, for cast stainless steels within ASTM Specification A 351, the saturation RT impact energy can be as low as 30, 25, and 20 J/cm^2 (≈12, 15, and 18 ft·lb) for CF–3, CF–8, and CF–8M steels, respectively. The lower–bound J–R curve for different grades of steel and temperature can be determined from Eqs. 18–22. The lower–bound values of C and n for

aged cast stainless steels are given in Table 4 and the J–R curves for static– and centrifugally cast CF–3, CF–8, and CF–8M are shown in Figs. 17 and 18.

The cast stainless steels used in the U.S. nuclear industry generally contain <15% ferrite. The lower–bound J–R curves shown in Figs. 17 and 18 are based on the "worst case" chemical composition (>20% ferrite) and are thus very conservative for most steels. Less conservative estimates of lower–bound J–R curves can be obtained if the ferrite content of the steel is known. The ferrite content of a cast stainless steel component can be measured in the field with a ferrite scope and a remote probe. The values of material parameter Φ in Eqs. 4 and 6 can be scaled with respect to the measured ferrite content to obtain more realistic estimates of saturation Charpy–impact energy and J–R curves for the material. The values of coefficient C and exponent n representing the lower–bound J–R curve for aged cast stainless steels with 10–15% ferrite and <10% ferrite, respectively, are given in Table 4. This information may be used as a guideline for establishing the upper limit of ferrite content for a specific grade of steel beyond which thermal aging effects are significant. For example, the results indicate that static– or centrifugally cast CF–3 and CF–8 steels with <10% ferrite would have adequate impact strength and fracture toughness even in the fully embrittled condition.

8 Procedure for Estimating Mechanical Properties

A flow diagram of the sequential steps required for estimating fracture toughness J–R curve, J_{IC}, tensile flow stress, and Charpy–impact energy is shown in Fig. 19. In Section A of the flow diagram, "lower–bound" fracture toughness J–R curves for cast stainless steels of unknown chemical composition are defined. Different lower–bound J–R curves are defined when the ferrite content of the steel is known. Sections B and C of the flow diagram present procedures for estimating mechanical properties when some information is known about the material, e.g., CMTR, is available. Section B describes the estimation of "saturation" impact energy and J–R curve, i.e., the lowest value that would be achieved for the material after long–term service. The only information needed for these estimations is the chemical composition of the material. Nitrogen content is assumed to be 0.04 wt.% if not known. The lower–bound J–R curve for unaged cast stainless steels is used as the saturation J–R curve of a material when the J–R curve estimated from the chemical composition is higher. Additional information, e.g., J–R curve of the unaged material or RT Charpy impact energy of unaged material for estimating fracture toughness, is required to justify the use of higher J–R curves.

Estimation of mechanical properties at any given time and temperature of service, is described in Section C of the flow diagram. The initial impact energy and flow stress of the unaged material and the constant θ are also required for these estimations. The value of θ depends on the service temperature; it is assumed to be 3.3 for temperatures <280°C (<536°F), 2.9 for temperatures of 280–330°C (536–626°F), and 2.5 for temperatures of 330–360°C (626–680°F). The initial impact energy of the unaged material can be assumed to be 200 J/cm^2 if not known. However, the lower–bound J–R curve for the unaged cast stainless steels is used when the J–R curve estimated from the chemical composition is higher than the lower bound for the unaged steel. The J_{IC} value is determined from the estimated J–R curve and flow stress.

9 Conclusions

A procedure and correlations are presented for predicting Charpy-impact energy, tensile flow stress, fracture toughness J-R curve, and J_{IC} value of aged cast stainless steels (ASTM A 351) from known material information. Mechanical properties of a specific cast stainless steel are estimated from the extent and kinetics of thermal embrittlement. Embrittlement of cast stainless steels is characterized in terms of RT Charpy-impact energy. The extent or degree of thermal embrittlement at "saturation," i.e., the minimum impact energy that can be achieved for the material after long-term aging, is determined from the chemical composition of the steel. The results indicate that Charpy-impact energy can be <50 J/cm^2 (<30 ft·lb) for cast stainless steels with ferrite contents as low as 10%.

Charpy-impact energy as a function of time and temperature of reactor service is estimated from the kinetics of thermal embrittlement, which is also determined from the chemical composition. The initial impact energy of the unaged steel is required for these estimations. Initial tensile flow stress is needed for estimating the flow stress of aged material. The fracture toughness J-R curve for the material is then obtained from correlations between RT Charpy-impact energy and fracture toughness parameters. The J_{IC} value is determined from the estimated J-R curve and flow stress. A common "lower-bound" J-R curve for cast stainless steels with unknown chemical composition is also defined for a given grade of steel, ferrite content, and temperature. This information can serve as a guideline for establishing the upper limit of ferrite content for a specific grade of steel beyond which thermal aging effects are significant.

Fracture toughness J-R curve data have been mostly obtained on 1-T compact tension specimens. According to ASTM Specification E 1152-87 they are valid only for crack growth up to 10% of the initial uncracked ligament. However, it is widely accepted that the J-R curve crack growth validity limits fall between 25 and 40% of the initial uncracked ligament, or ≈8 mm of crack extension. In future work under this program, these extended validity limits for J-controlled crack growth will be qualified and better defined for cast stainless steels in terms of specimen size, toughness, and crack extension. Representation of J-R curves by expressions other than power law (e.g., by power-exponential relation) will also be evaluated for more accurate extrapolation of J-R curve data.

Acknowledgments

This work was supported by the Office of Nuclear Regulatory Research of the U.S. Nuclear Regulatory Commission. The author thanks A. Sather, T. M. Galvin, L. Y. Bush, W. F. Michaud, and W. F. Burke for experimental contributions and J. Muscara, W. J. Shack, and T. F. Kassner for their helpful discussions.

References

1. O. K. Chopra and H. M. Chung, Aging Degradation of Cast Stainless Steels: Effects on Mechanical Properties, in: Environmental Degradation of Materials in Nuclear Power Systems-Water Reactors, eds. G. J. Theus and J. R. Weeks (The Metallurgical Society, Warrendale, PA., 1988) pp. 737-748.

2. O. K. Chopra and H. M. Chung, Effect of Low-Temperature Aging on the Mechanical Properties of Cast Stainless Steels, in: Properties of Stainless Steels in Elevated Temperature Service, ed. M. Prager, MPC Vol. 26, PVP Vol. 132 (American Society of Mechanical Engineers, New York, 1988) pp. 79–105.

3. O. K. Chopra, Thermal Aging of Cast Stainless Steels: Mechanisms and Predictions, in: Fatigue, Degradation, and Fracture – 1990, eds. W. H. Bamford, C. Becht, S. Bhandari, J. D. Gilman, L. A. James, and M. Prager, MPC Vol. 30, PVP Vol. 195 (American Society of Mechanical Engineers, New York, 1990) pp. 193-214.

4. O. K. Chopra and A. Sather, Initial Assessment of the Mechanisms and Significance of Low-Temperature Embrittlement of Cast Stainless Steels in LWR Systems, NUREG/CR-5385, ANL-89/17, Argonne National Laboratory, Argonne, IL (August 1990).

5. A. Trautwein and W. Gysel, Influence of Long Time Aging of CF-8 and CF-8M Cast Steel at Temperatures Between 300 and 500°C on the Impact Toughness and the Structure Properties, in: Stainless Steel Castings, eds. V. G. Behal and A. S. Melilli, ASTM STP 756 (American Society for Testing and Materials, Philadelphia, PA, 1982) pp. 165–189.

6. E. I. Landerman and W. H. Bamford, Fracture Toughness and Fatigue Characteristics of Centrifugally Cast Type 316 Stainless Steel Pipe after Simulated Thermal Service Conditions, in: Ductility and Toughness Considerations in Elevated Temperature Service, MPC-8 (American Society of Mechanical Engineers, New York, 1978) pp. 99–127.

7. S. Bonnet, J. Bourgoin, J. Champredonde, D. Guttmann, and M. Guttmann, Relationship between Evolution of Mechanical Properties of Various Cast Duplex Stainless Steels and Metallurgical and Aging Parameters: An Outline of Current EDF Programmes, Mater. Sci. and Technol. 6 (1990) 221–229.

8. K. N. Akhurst and P. H. Pumphrey, The Aging Kinetics of CF3 Cast Stainless Steel in the Temperature Range 300°C to 400°C, RD/L/3354/R88, Central Electricity Generating Board, Leatherhead, UK (November 1988).

9. P. H. Pumphrey and K. N. Akhurst, Aging Kinetics of CF3 Cast Stainless Steel in Temperature Range 300 – 400°C, Mater. Sci. and Technol. 6 (1990) 211–219.

10. G. Slama, P. Petrequin, and T. Mager, Effect of Aging on Mechanical Properties of Austenitic Stainless Steel Castings and Welds, presented at SMIRT Post-Conference Seminar 6, Assuring Structural Integrity of Steel Reactor Pressure Boundary Components, Monterey, CA (August 29–30, 1983).

11. Y. Meyzaud, P. Ould, P. Balladon, M. Bethmont, and P. Soulat, Tearing Resistance of Aged Cast Austenitic Stainless Steel, presented at Intl. Conf. on Thermal Reactor Safety (NUCSAFE 88), Avignon, France (October 1988).

12. P. McConnell and J. W. Sheckherd, Fracture Toughness Characterization of Thermally Embrittled Cast Duplex Stainless Steel, Report NP-5439, Electric Power Research Institute, Palo Alto, CA. (September 1987).

13. O. K. Chopra, Estimation of Fracture Toughness of Cast Stainless Steels in LWR Systems, in: Proc. 18th Water Reactor Safety Information Meeting, NUREG/CP-0114 Vol. 3 (U.S. Nuclear Regulatory Commission, April 1991) p. 195.

14. O. K. Chopra, Estimation of Fracture Toughness of Cast Stainless Steels during Thermal Aging in LWR Systems, NUREG/CR-4513, ANL-90/42, Argonne National Laboratory, Argonne, IL (June 1991).

15. M. Vrinat, R. Cozar, and Y. Meyzaud, Precipitated Phases in the Ferrite of Aged Cast Duplex Stainless Steels, Scripta Metal., 20 (1986) 1101-1106.

16. H. M. Chung, Thermal Aging of Decommissioned Reactor Cast Stainless Steel Components and Methodology for Life Prediction, in: Life Assessment and Life Extension of Power Plant Components, eds. T. V. Narayanan, C. B. Bond, J. Sinnappan, A. E. Meligi, M. Prager, T. R. Mager, J. D. Parker, and K. Means, PVP Vol. 171 (American Society of Mechanical Engineers, New York, 1989) pp. 111-125.

17. H. M. Chung and T. R. Leax, Embrittlement of Laboratory and Reactor Aged CF3, CF8, and CF8M Duplex Stainless Steels, Mater. Sci. and Tech. 6 (1990) 249-262.

18. J. Sassen, M. G. Hetherington, T. J. Godfrey, G. D. W. Smith, P. H. Pumphrey, and K. N. Akhurst, Kinetics of Spinodal Reaction in the Ferrite Phase of a Duplex Stainless Steel, in: Properties of Stainless Steels in Elevated Temperature Service, ed. M. Prager, MPC Vol. 26, PVP Vol. 132 (American Society of Mechanical Engineers, New York, 1988) pp. 65-78.

19. M. K. Miller and J. Bentley, Characterization of Fine-Scale Microstructures in Aged Primary Coolant Pipe Steels, in: Environmental Degradation of Materials in Nuclear Power Systems-Water Reactors, Proc. 3rd Intl. Symp., eds. G. J. Theus and J. R. Weeks (The Metallurgical Society, Warrendale, PA., 1988) pp. 341-349.

20. P. Auger, F. Danoix, A. Menand, S. Bonnet, J. Bourgoin, and M. Guttmann, Atom Probe and Transmission Electron Microscopy Study of Aging of Cast Duplex Stainless Steels, Mater. Sci. and Technol. 6 (1990) 301-313.

21. J. E. Brown, A. Cerezo, T. J. Godfrey, M. G. Hetherington, and G. D. W. Smith, Quantitative Atom Probe Analysis of Spinodal Reaction in Ferrite Phase of Duplex Stainless Steel, Mater. Sci. and Technol. 6 (1990) 293-300.

22. L. S. Aubrey, P. F. Wieser, W. J. Pollard, and E. A. Schoefer, Ferrite Measurement and Control in Cast Duplex Stainless Steel, in: Stainless Steel Castings, eds. V. G. Behal and A. S. Melilli, ASTM STP 756 (American Society for Testing and Materials, Philadelphia, PA, 1982) pp. 126-164.

23. A. L. Hiser, Tensile and J-R Curve Characterization of Thermally Aged Cast Stainless Steels, NUREG/CR-5024, MEA-2229, Materials Engineering Associates, Inc., Lanham, MD, (September 1988).

24. G. E. Hale and S. J. Garwood, The Effect of Aging on the Fracture Behaviour of Cast Stainless Steel and Weldments, Mater. Sci. and Technol. 6 (1990) 230-235.

25. A. L. Hiser, Fracture Toughness Characterization of Nuclear Piping Steels, NUREG/CR-5118, MEA-2325, Materials Engineering Associates, Inc., Lanham, MD, (November 1989).

26. G. M. Wilkowski, et. al., Degraded Piping Program - Phase II, Semiannual Report, NUREG/CR-4082, Vol. 2 (June 1985).

27. W. J. Mills, Heat-to-Heat Variations in the Fracture Toughness of Austenitic Stainless Steels, Eng. Fracture Mech. 30 (1988) 469–492.

28. M. G. Vassilaros, R. A. Hays, and J. P. Gudas, Investigation of the Ductile Fracture Properties of Type 304 Stainless Steel Plate, Welds, and 4–Inch Pipe, in: Proc. 12th Water Reactor Safety Information Meeting, NUREG/CP–0058 Vol. 4 (U.S. Nuclear Regulatory Commission, January 1985) p. 176.

29. P. Balladon, J. Heritier, and P. Rabbe, Influence of Microstructure on the Ductile Rupture Mechanisms of a 316L Steel at Room and Elevated Temperatures, in: Fracture Mechanics: Fourteenth Symposium, ASTM STP 791 (1983) pp. II496–II513.

30. W. H. Bamford and A. J. Bush, Fracture Behavior of Stainless Steel, in: Elastic–Plastic Fracture, ASTM STP 668, (1979) pp. 553–577.

Table 1. Chemical composition, ferrite content, and kinetics of thermal embrittlement for various heats of cast stainless steels

	Chemical Composition (wt.%)							Ferrite (%)		$C_{V_{sat}}$	Constants			Q
Heat	Cr	Mo	Si	Ni	Mn	C	N	Calc.	Meas.	(J/cm^2)	β	θ	α	(kJ/mole)
Argonne														
52	19.49	0.35	0.92	9.40	0.57	0.009	0.052	10.3	13.5	161.8	–	–	–	–
51	20.13	0.32	0.86	9.06	0.63	0.010	0.058	14.3	18.0	115.9	0.139	3.53	1.15	204.7
47	19.81	0.59	1.06	10.63	0.60	0.018	0.028	8.4	16.3	163.7	0.069	2.29	1.20	195.7
P2	20.20	0.16	0.94	9.38	0.74	0.019	0.040	12.5	15.6	141.3	0.258	2.83	1.09	218.6
I	20.20	0.45	0.83	8.70	0.47	0.019	0.032	20.4	17.1	134.3	0.094	2.10	1.00	250.0
69	20.18	0.34	1.13	8.59	0.63	0.023	0.028	21.0	23.6	76.7	0.214	3.21	1.07	175.9
P1	20.49	0.04	1.12	8.10	0.59	0.036	0.057	17.6	24.1	53.7	0.305	2.57	0.75	252.7
61	20.65	0.32	1.01	8.86	0.65	0.054	0.080	10.0	13.1	93.3	0.214	3.48	1.20	197.8
59	20.33	0.32	1.08	9.34	0.60	0.062	0.045	8.8	13.5	89.1	0.197	3.14	1.20	249.4
68	20.64	0.31	1.07	8.08	0.64	0.063	0.062	14.9	23.4	47.1	0.301	2.88	0.68	161.1
60	21.05	0.31	0.95	8.34	0.67	0.064	0.058	15.4	21.1	44.8	0.291	2.89	0.88	210.9
56	19.65	0.34	1.05	9.28	0.57	0.066	0.030	7.3	10.1	117.6	–	–	–	–
74	19.11	2.51	0.73	9.03	0.54	0.064	0.048	15.5	18.4	63.1	0.269	3.44	0.70	95.0
75	20.86	2.58	0.67	9.12	0.53	0.065	0.052	24.8	27.8	32.1	0.436	2.82	0.51	139.0
66	19.45	2.39	0.49	9.28	0.60	0.047	0.029	19.6	19.8	8?.9	0.208	3.16	1.57	163.9
64	20.76	2.46	0.63	9.40	0.60	0.038	0.038	29.0	28.4	41.1	0.338	2.81	0.60	147.3
65	20.78	2.57	0.48	9.63	0.50	0.049	0.064	20.9	23.4	59.7	0.260	2.99	0.59	153.8
P4	19.64	2.05	1.02	10.00	1.07	0.040	0.151	5.9	10.0	62.7	0.289	2.70	0.62	158.7
63	19.37	2.57	0.58	11.85	0.61	0.055	0.031	6.4	10.4	126.5	0.119	2.83	1.11	155.5
Georg Fischer Co.														
284	23.00	0.17	0.52	8.23	0.28	0.025	0.037	43.6	42.0	23.8	0.560	3.71	0.41	87.4
280	21.60	0.25	1.37	8.00	0.50	0.028	0.038	36.3	38.0	24.4	0.591	3.30	0.73	86.7
282	22.50	0.15	0.35	8.53	0.43	0.035	0.040	29.7	38.0	30.2	0.525	3.73	0.43	97.8
281	23.10	0.17	0.45	8.60	0.41	0.036	0.053	31.4	30.0	26.6	0.560	3.76	0.42	92.6
283	22.60	0.23	0.53	7.88	0.48	0.036	0.032	42.6	42.0	23.8	0.580	3.65	0.43	82.9
278	20.20	0.13	1.00	8.27	0.28	0.038	0.030	18.5	15.0	67.6	0.381	4.05	0.47	62.7
279	22.00	0.22	1.36	7.85	0.37	0.040	0.032	39.5	40.0	23.8	0.586	3.21	0.69	91.8
277	20.50	0.06	1.81	8.13	0.54	0.052	0.019	22.5	28.0	33.9	0.488	3.65	0.55	87.7
291	19.60	0.66	1.59	10.60	0.28	0.065	0.054	4.2	6.0	123.0	0.235	3.89	0.79	77.5
292	21.60	0.13	1.57	7.52	0.34	0.090	0.039	23.9	28.0	22.4	0.392	3.08	0.46	99.3
290	20.00	2.40	1.51	8.30	0.41	0.054	0.050	31.3	32.0	21.1	0.602	3.49	0.11	81.0
288	19.60	2.53	1.70	8.40	0.47	0.052	0.022	35.6	28.0	19.4	0.643	3.02	0.64	106.1
287	20.50	2.58	0.51	8.46	0.50	0.047	0.033	37.2	38.0	23.8	0.563	3.52	0.42	91.6
286	20.20	2.44	1.33	9.13	0.40	0.072	0.062	18.9	22.0	20.5	0.571	3.11	0.62	105.5
289	19.70	2.30	1.44	8.25	0.48	0.091	0.032	22.6	30.0	20.9	0.571	3.32	0.39	90.4
285	18.80	2.35	0.86	9.49	0.48	0.047	0.039	14.0	10.0	64.3	0.347	3.76	0.34	82.0
Framatome														
A	18.90	0.10	0.99	8.90	1.14	0.021	0.074	6.0	6.3	166.0	0.090	3.44	0.20	111.7
E	21.04	0.08	0.54	8.47	0.80	0.035	0.051	17.6	16.5	45.7	0.334	2.63	0.65	132.9
F	19.72	0.34	1.16	8.33	0.26	0.038	0.026	17.7	12.0	83.2	0.282	2.45	1.23	176.2
C	20.73	0.13	1.09	8.19	0.91	0.042	0.035	20.9	20.1	51.1	0.393	3.30	0.45	83.1
G	20.65	0.02	1.03	8.08	0.74	0.040	0.073	15.3	17.0	62.5	–	–	–	–
H	20.70	0.05	1.18	8.07	0.71	0.050	0.045	18.3	21.5	50.6	–	–	–	–
D	19.15	2.50	0.94	10.32	1.12	0.026	0.063	12.2	13.9	33.0	0.439	3.30	0.40	99.7
I	19.36	2.40	0.98	10.69	0.70	0.020	0.039	14.1	15.5	150.7	–	–	–	–
K	20.80	2.62	0.75	10.45	1.09	0.060	0.056	15.4	14.0	48.5	–	–	–	–
L	20.76	2.48	0.81	10.56	0.79	0.040	0.042	18.6	19.0	30.4	–	3.00	–	–
B	20.12	2.52	0.93	10.56	0.83	0.053	0.042	14.0	17.3	28.2	0.478	2.55	0.47	128.6
Westinghouse														
C1488	20.95	2.63	0.53	9.48	1.02	0.061	0.056	22.1	14.0	53.1	–	2.80	–	–
Electric Power Research Institute														
EPRI	22.04	0.23	0.84	7.93	0.74	0.030	0.045	36.0	32.0	30.0	0.564	2.10	0.60	–

Table 2. Values of the constants in Eq. 17 for estimating tensile flow stress of aged cast stainless steels

	Room Temp.			290–320°C		
Grade	a_1	b_1	c_1	a_1	b_1	c_1
CF-3	0.94	0.047	1.10	0.89	0.059	1.08
CF-8	0.90	0.074	1.16	0.87	0.088	1.14
CF-8M	0.80	0.101	1.19	0.71	0.143	1.24

Table 3. Values of the constants in Eq. 22 for estimating exponent n of the power-law J-R curve for cast stainless steels

	Room Temp.		290–320°C	
Grade	a_2	b_2	a_2	b_2
CF-3	0.08	0.228	0.14	0.130
CF-8	0.22	0.139	0.22	0.074
CF-8M	0.25	0.077	0.23	0.057

Table 4. Values of the coefficient C and exponent n for the lower bound J-R curve for cast stainless steels

			Static-Cast				Centrifugally Cast			
		C_V	Room Temp.		290°C		Room Temp.		290°C	
Grade	ϕ	(J/cm^2)	C	n	C	n	C	n	C	n
Ferrite Content >15%										
CF-3	40	30	287	0.42	264	0.33	334	0.42	347	0.33
CF-8	48	25	261	0.41	251	0.32	304	0.41	330	0.32
CF-8M	40	20	119	0.35	167	0.30	149	0.35	195	0.30
Ferrite Content 10–15%										
CF-3	30	42	342	0.45	290	0.35	398	0.45	382	0.35
CF-8	36	34	307	0.42	274	0.33	357	0.43	360	0.33
CF-8M	32	28	149	0.36	192	0.31	186	0.36	223	0.31
Ferrite Content <10%										
CF-3	20	67	400	0.47	331	0.38	507	0.50	435	0.38
CF-8	24	55	394	0.46	313	0.35	458	0.46	412	0.35
CF-8M	24	47	211	0.38	238	0.33	264	0.38	276	0.33

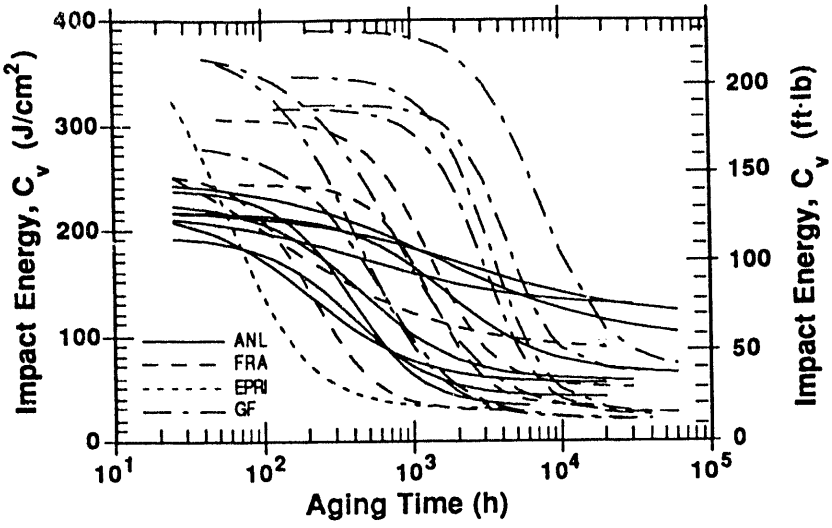

Figure 1. Decrease in Charpy-impact energy for various heats of cast stainless steels aged at 400°C

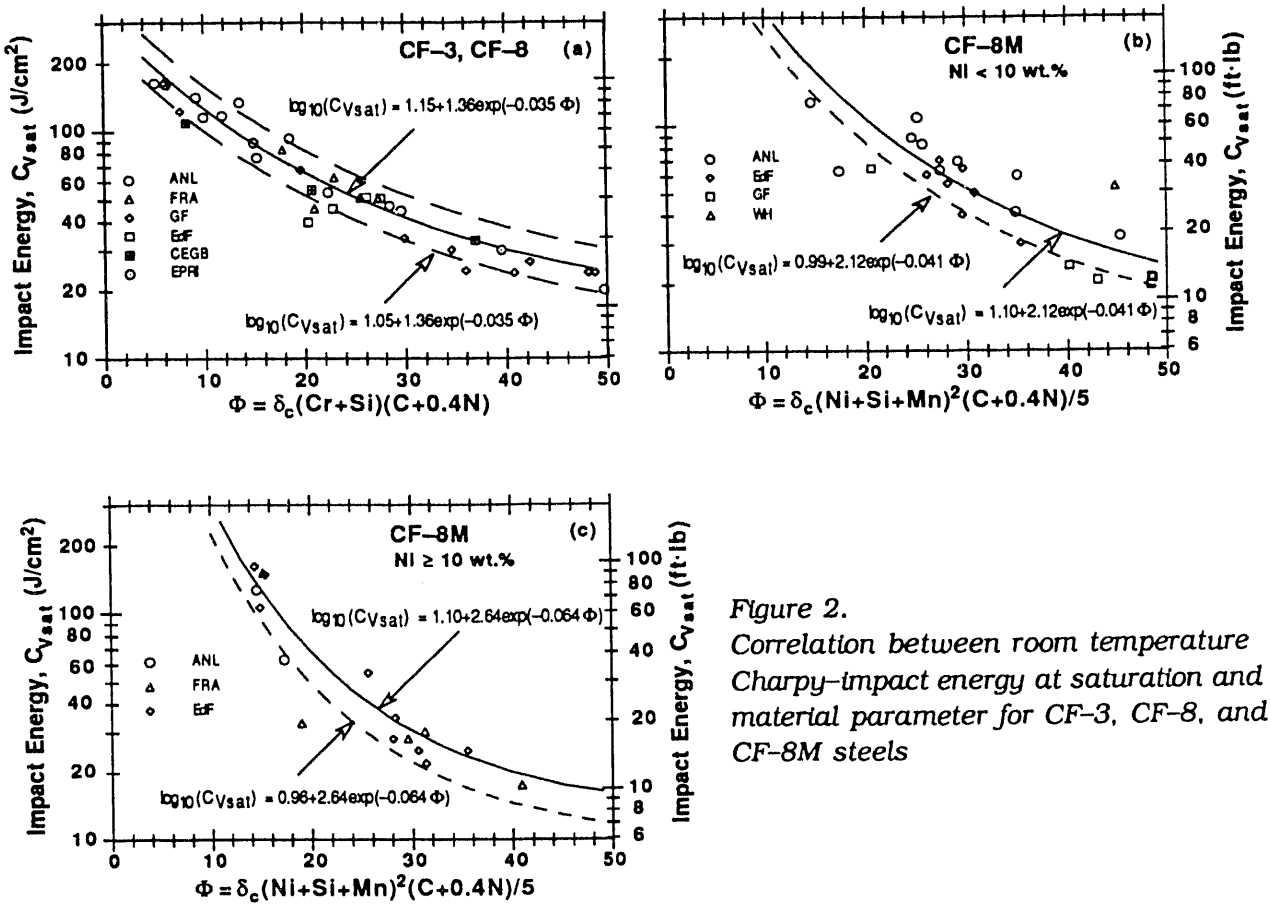

Figure 2. Correlation between room temperature Charpy-impact energy at saturation and material parameter for CF-3, CF-8, and CF-8M steels

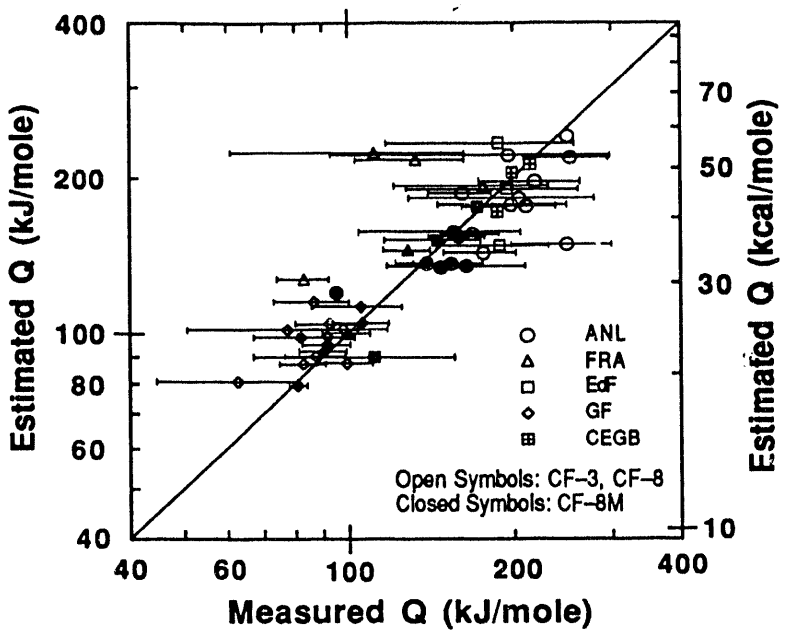

Figure 3. Observed and estimated activation energy for thermal embrittlement of cast stainless steels

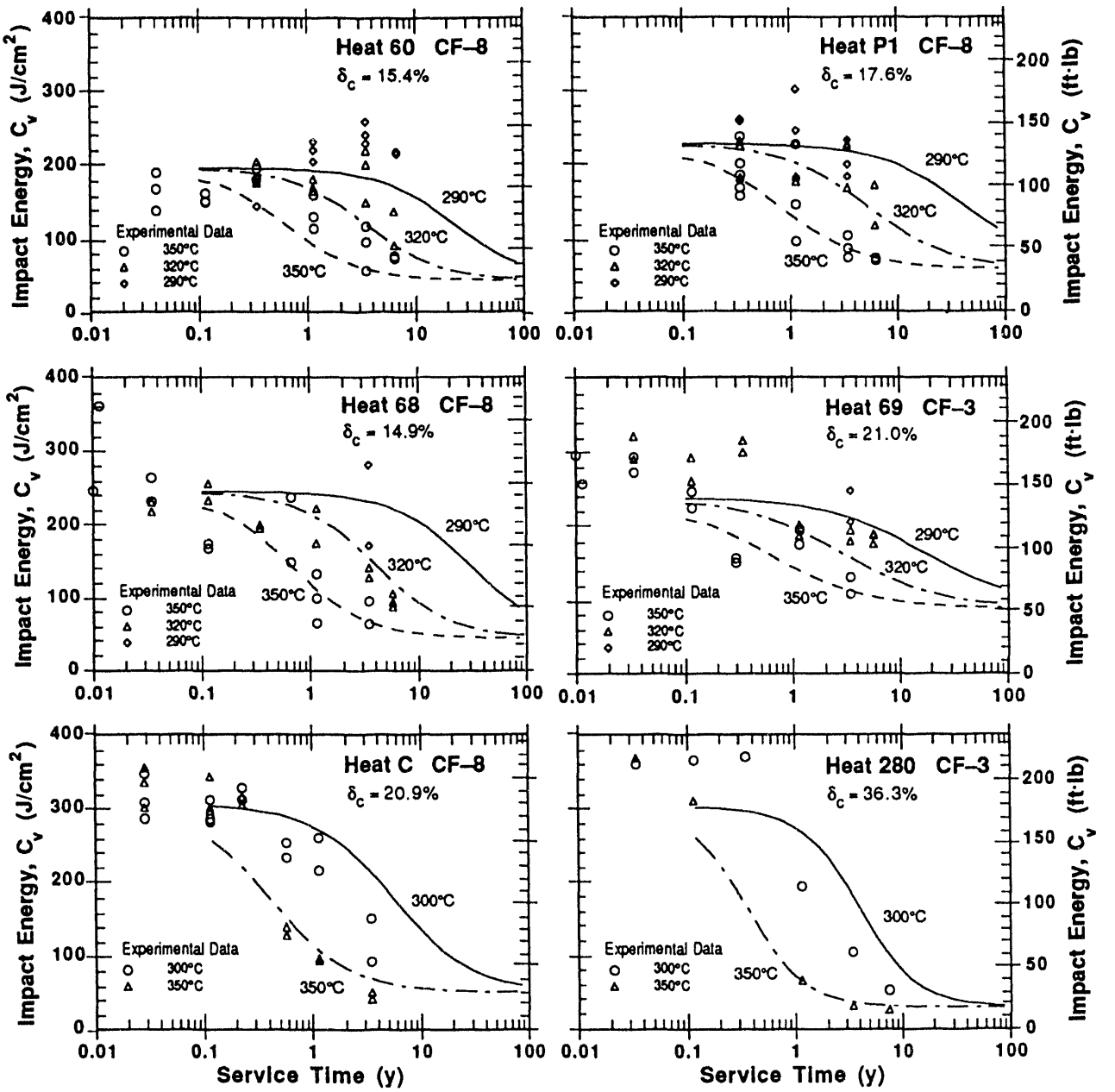

Figure 4. Room temperature Charpy-impact energy for aged CF-3 and CF-8 steels observed experimentally and that estimated from the composition and initial impact energy of the materials from ANL (Heats 60, 68, 69, and P1), FRA (Heat C), and GF (Heat 280) studies. δ_c is the calculated ferrite content.

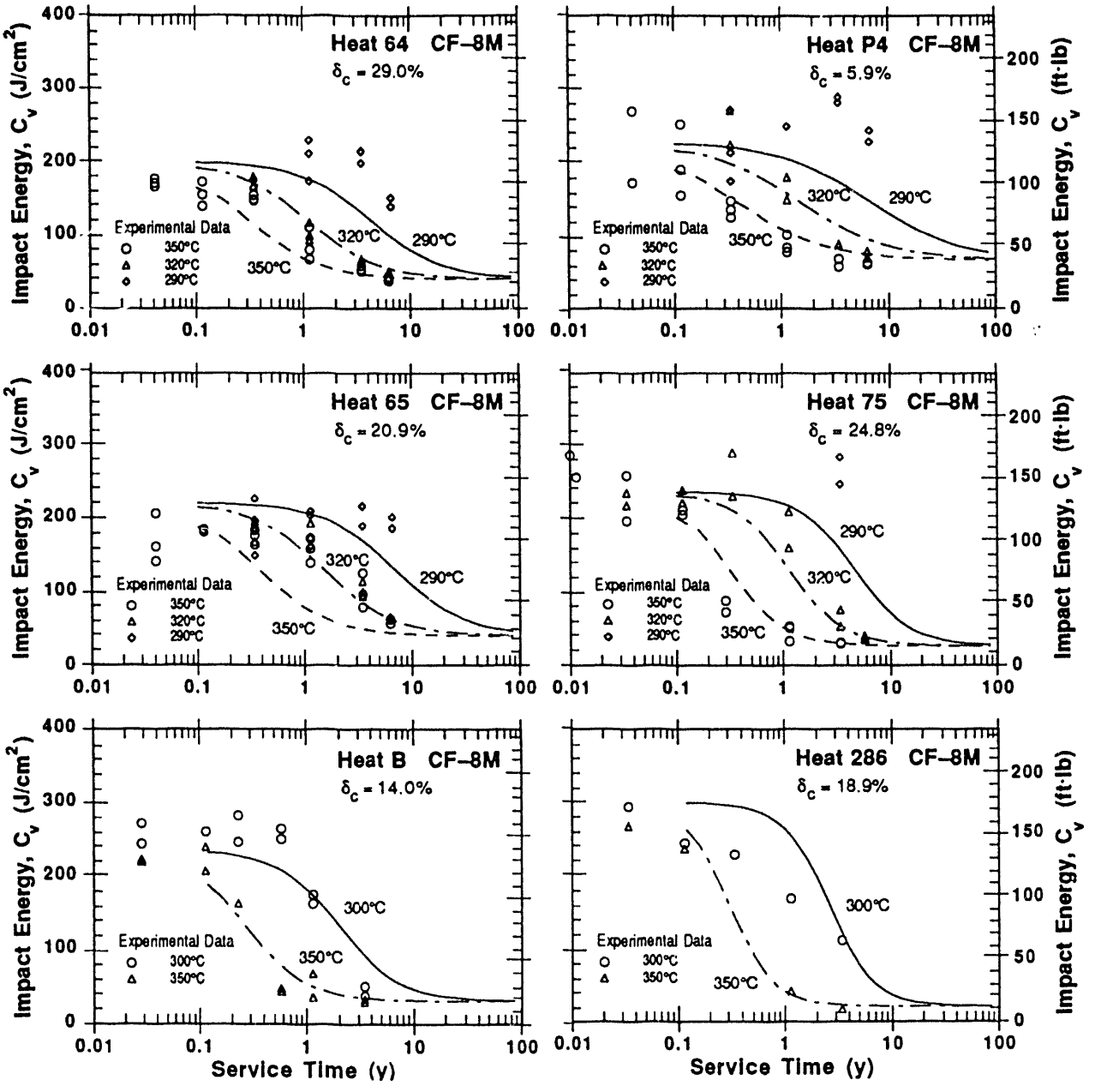

Figure 5. Room temperature Charpy-impact energy for aged CF-8M steels observed experimentally and that estimated from the composition and initial impact energy of the material from ANL (Heats 64, 65, 75, and P4), FRA (Heat B), and GF (Heat 286) studies. δ_c is the calculated ferrite content.

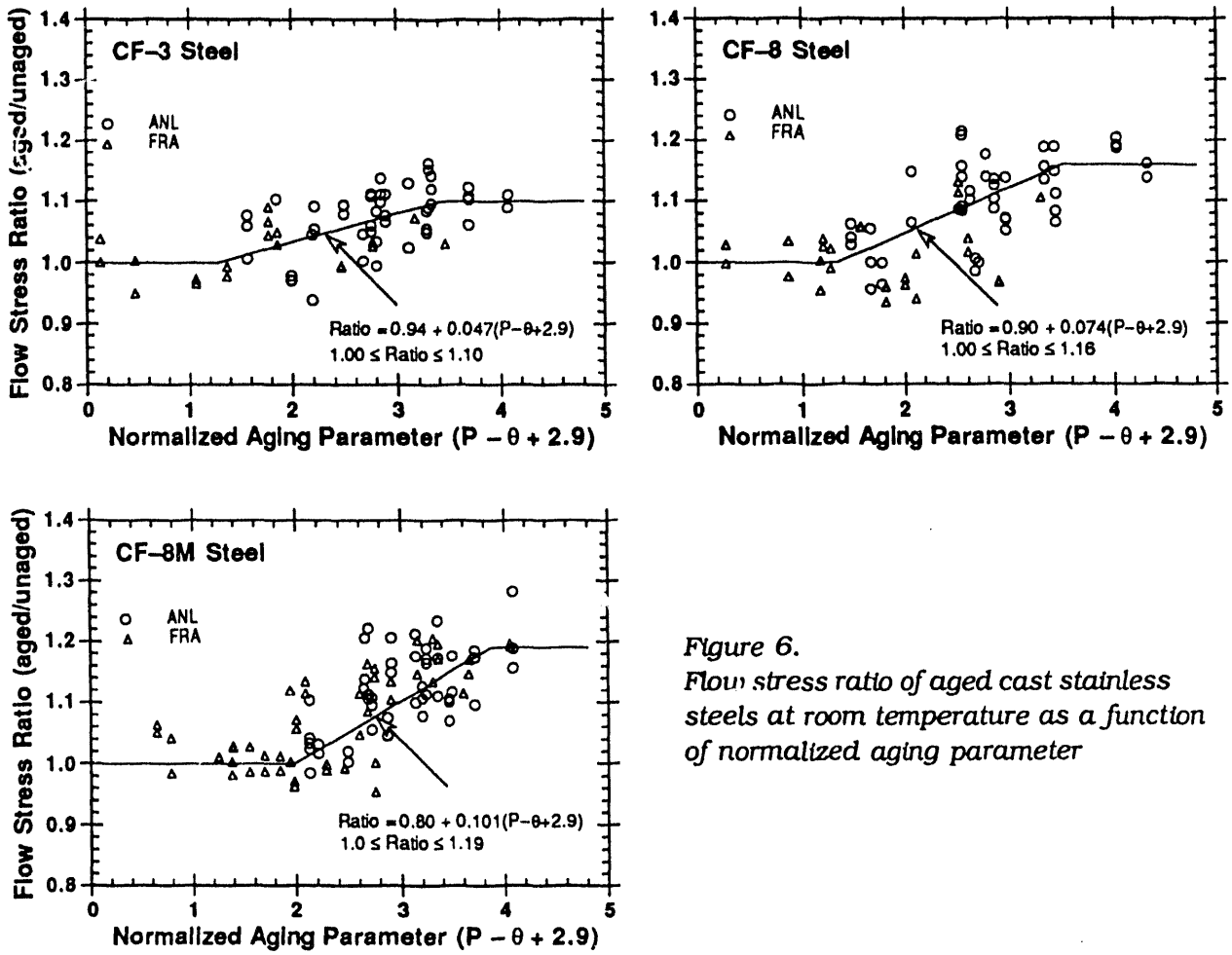

Figure 6.
Flow stress ratio of aged cast stainless steels at room temperature as a function of normalized aging parameter

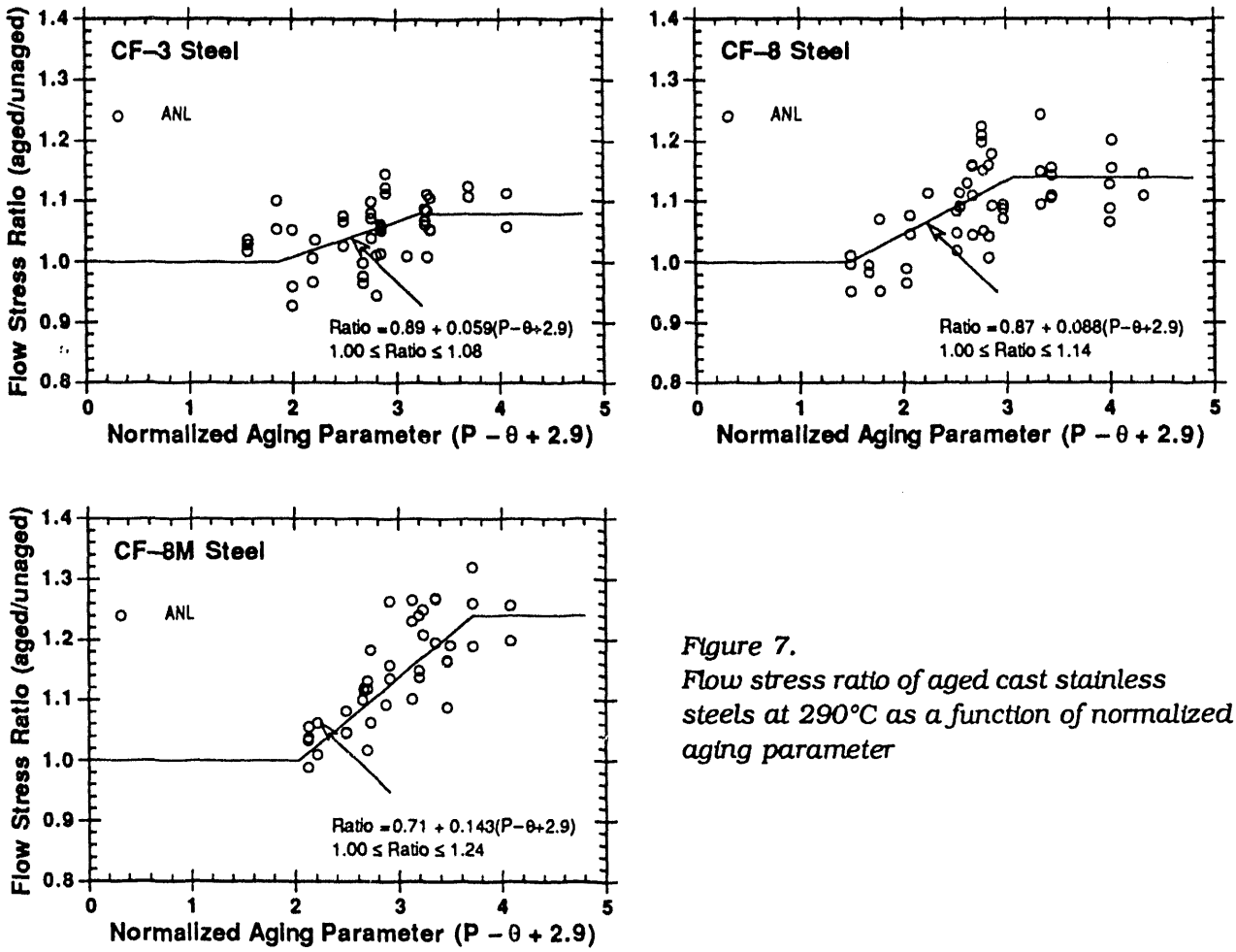

Figure 7.
Flow stress ratio of aged cast stainless steels at 290°C as a function of normalized aging parameter

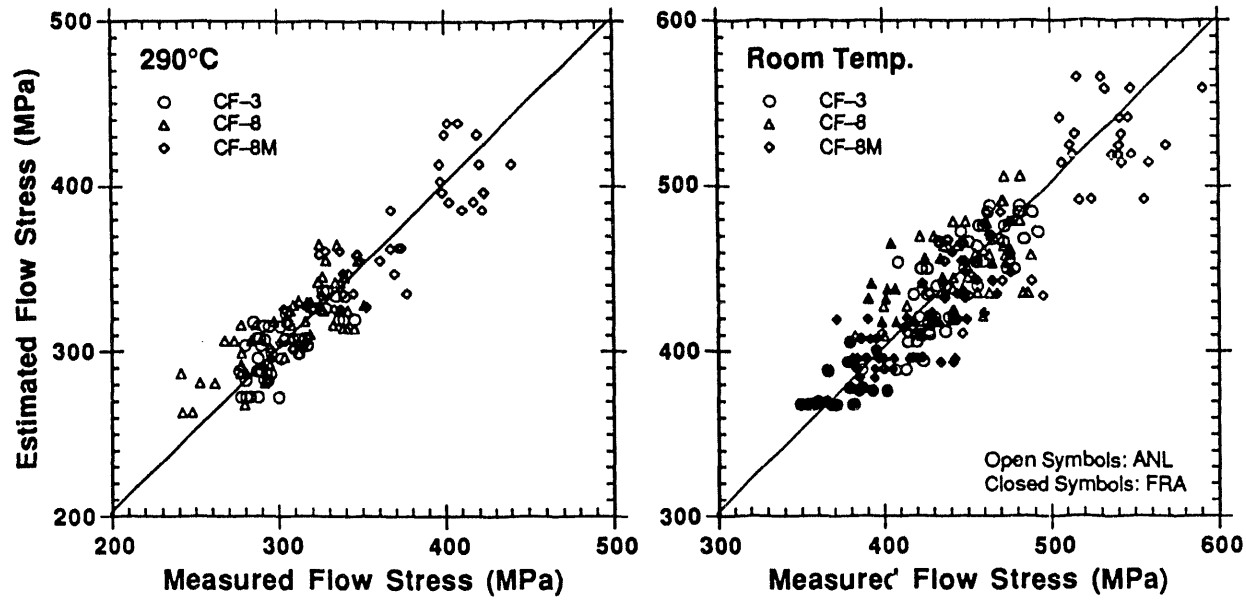

Figure 8. Observed and estimated flow stress of aged cast stainless steel at 290°C and room temperature

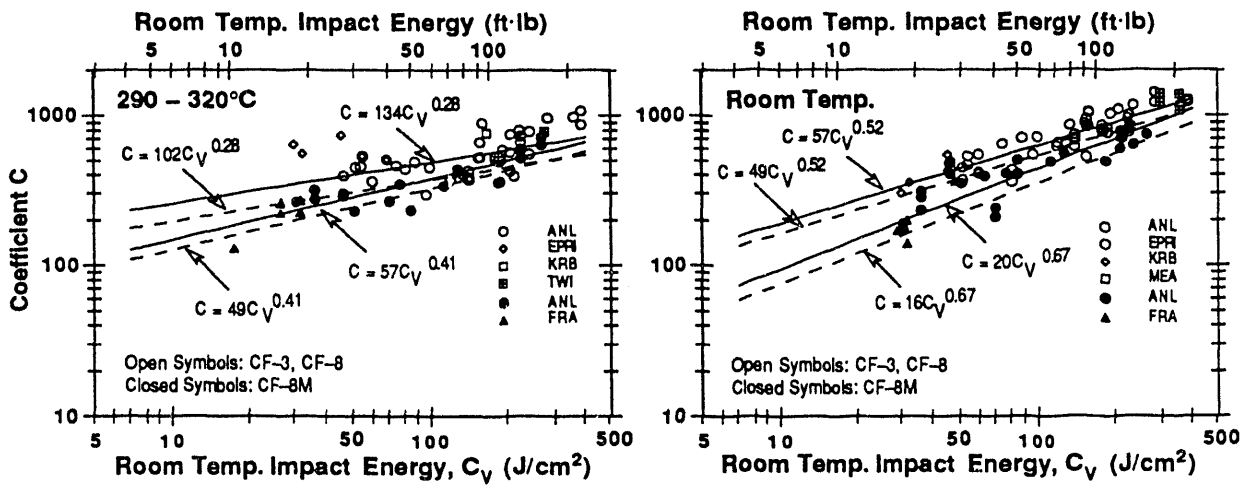

Figure 9. Correlation between RT Charpy-impact energy and coefficient C for cast stainless steel at 290–320°C and at room temperature. The solid and dashed lines represent the correlations used to estimate the J-R curves for centrifugally and static-cast materials, respectively.

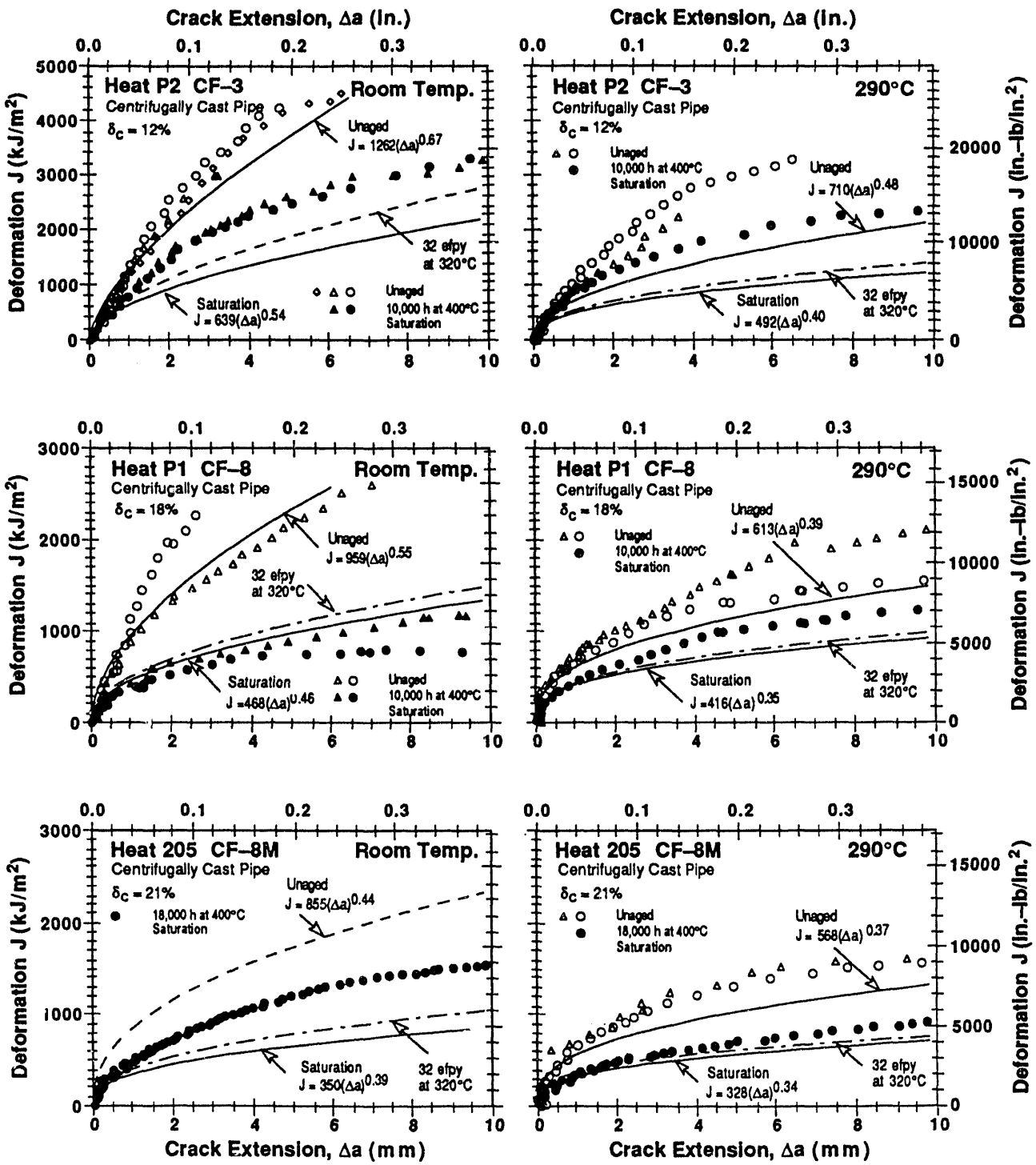

Figure 10. Saturation fracture toughness J-R curves at RT and 290°C estimated from the chemical composition of centrifugally cast CF-3, CF-8, and CF-8M pipes, and determined experimentally. δ_c is the calculated ferrite content.

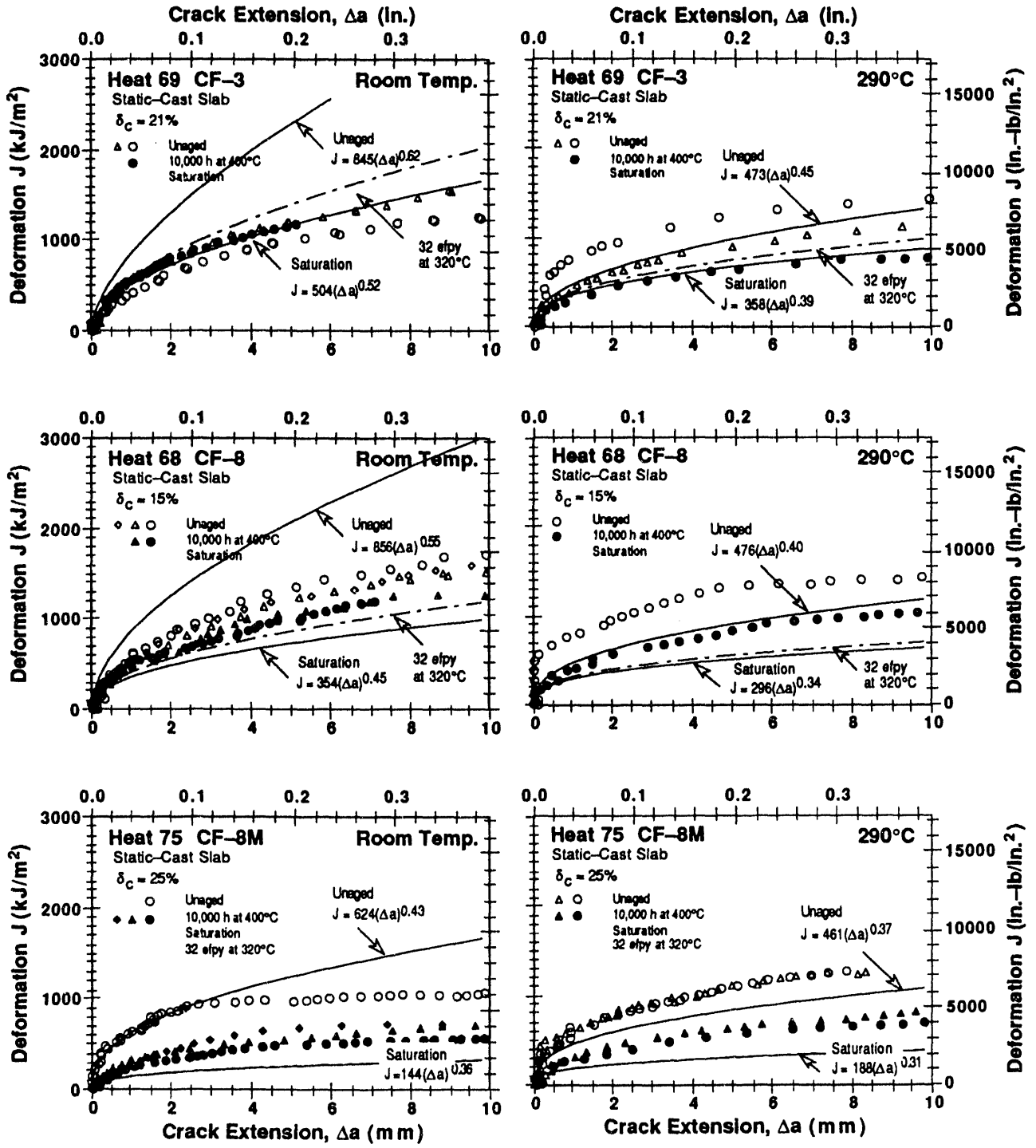

Figure 11. Saturation fracture toughness J-R curves at RT and 290°C estimated from the chemical composition of static-cast CF-3, CF-8, and CF-8M slabs, and determined experimentally. δ_c is the calculated ferrite content.

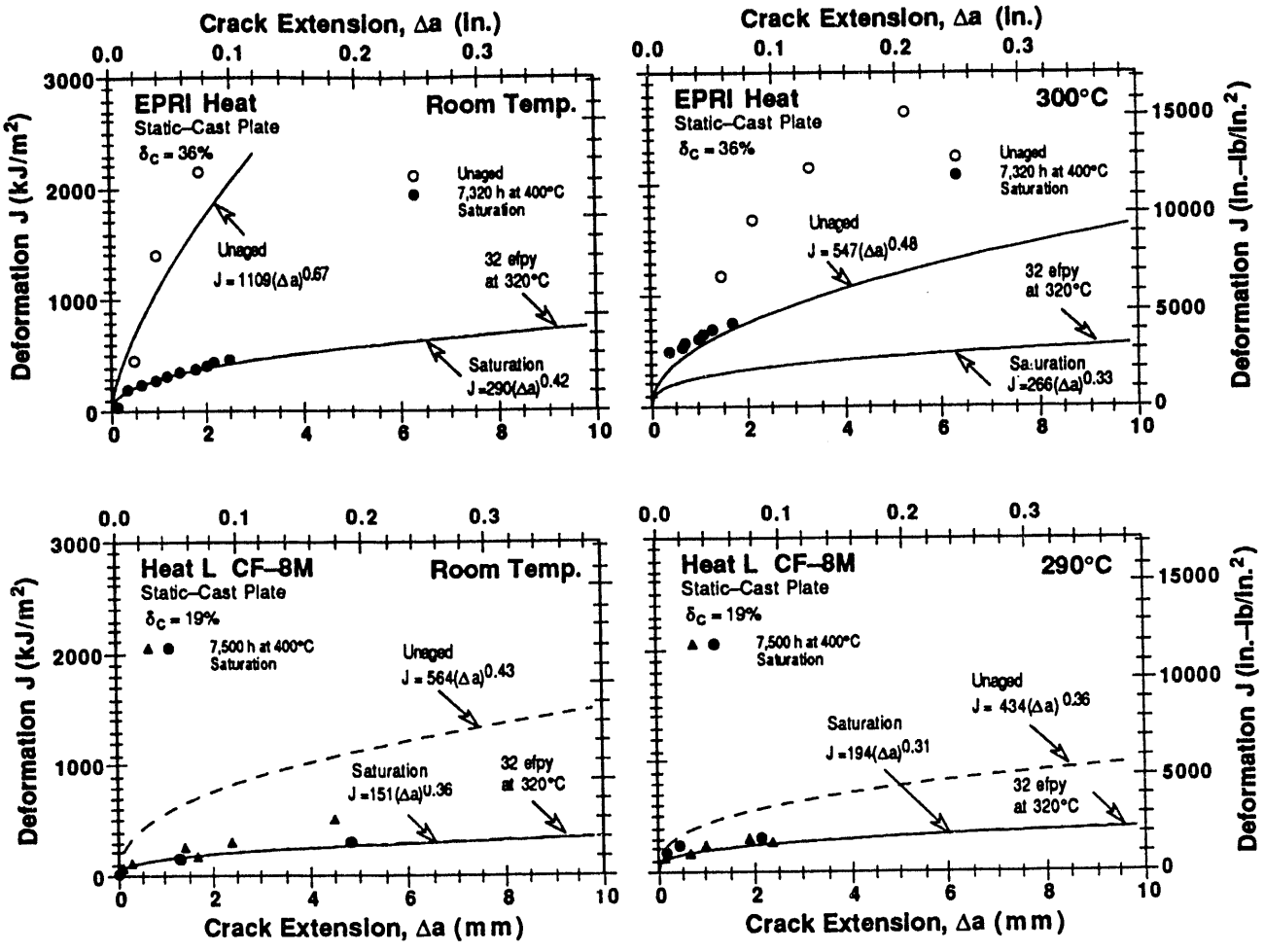

Figure 12. Saturation fracture toughness J-R curves at RT and 290°C estimated from the chemical composition of static-cast CF-3 and CF-8M plates (Refs. 10, 12), and determined experimentally. δ_c is the calculated ferrite content.

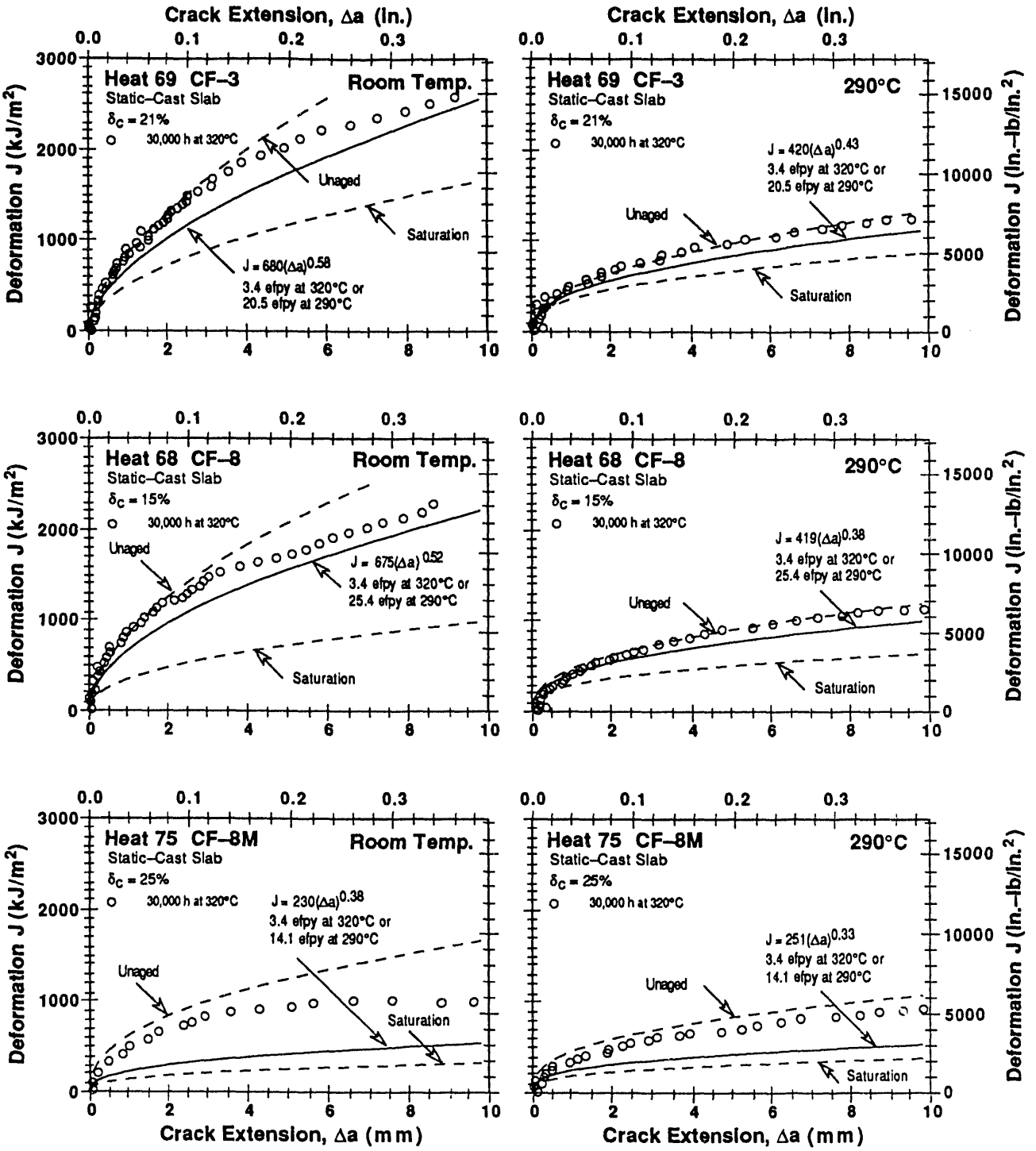

Figure 13. Fracture toughness J-R curves at room temperature and 290°C, estimated from the chemical composition and initial Charpy-impact energy and determined experimentally for partially aged static-cast CF-3, CF-8, and CF-8M slabs. δ_c is the calculated ferrite content.

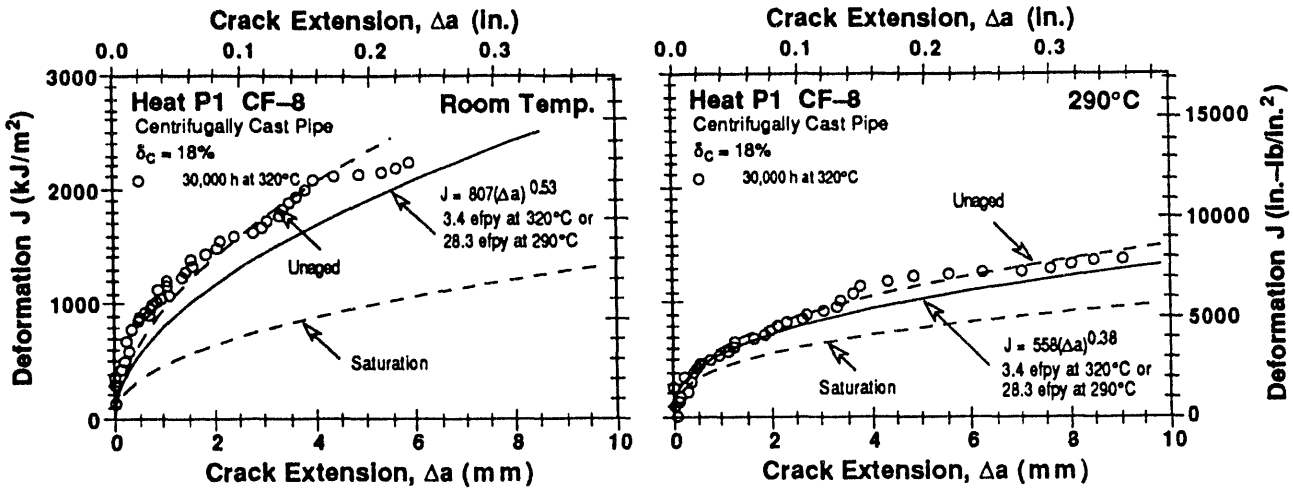

Figure 14. Fracture toughness J-R curve at room temperature and 290°C, estimated from the chemical composition and initial Charpy-impact energy and determined experimentally for partially aged centrifugally cast CF-8 pipe. δ_c is the calculated ferrite content.

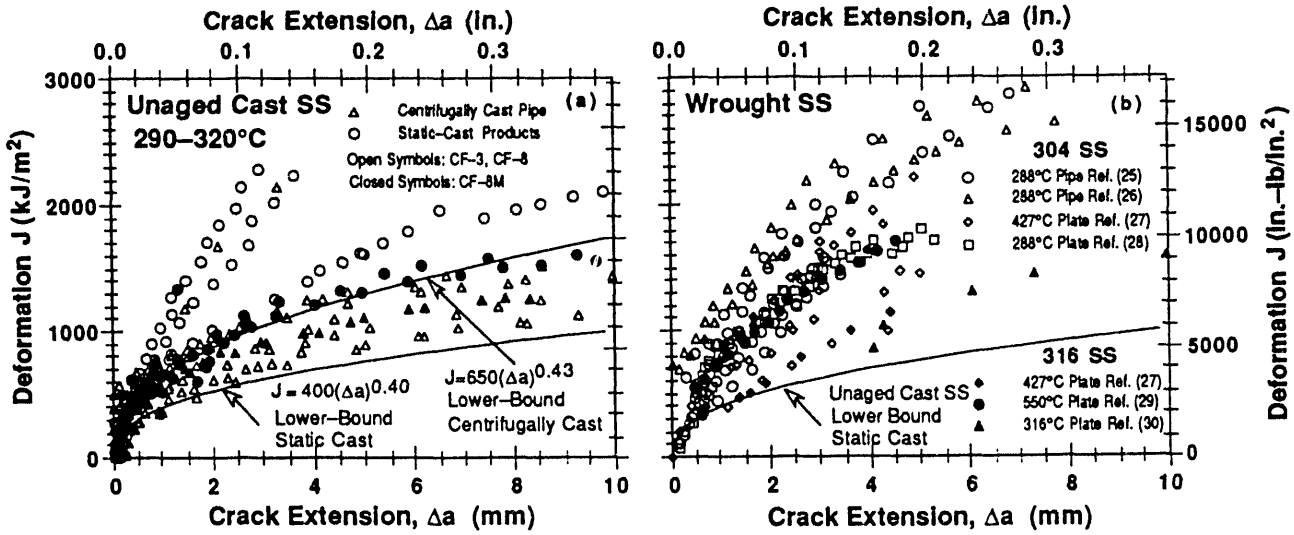

Figure 15. Fracture toughness J-R curve for (a) unaged cast stainless steels and (b) wrought stainless steels at temperatures ≥290°C

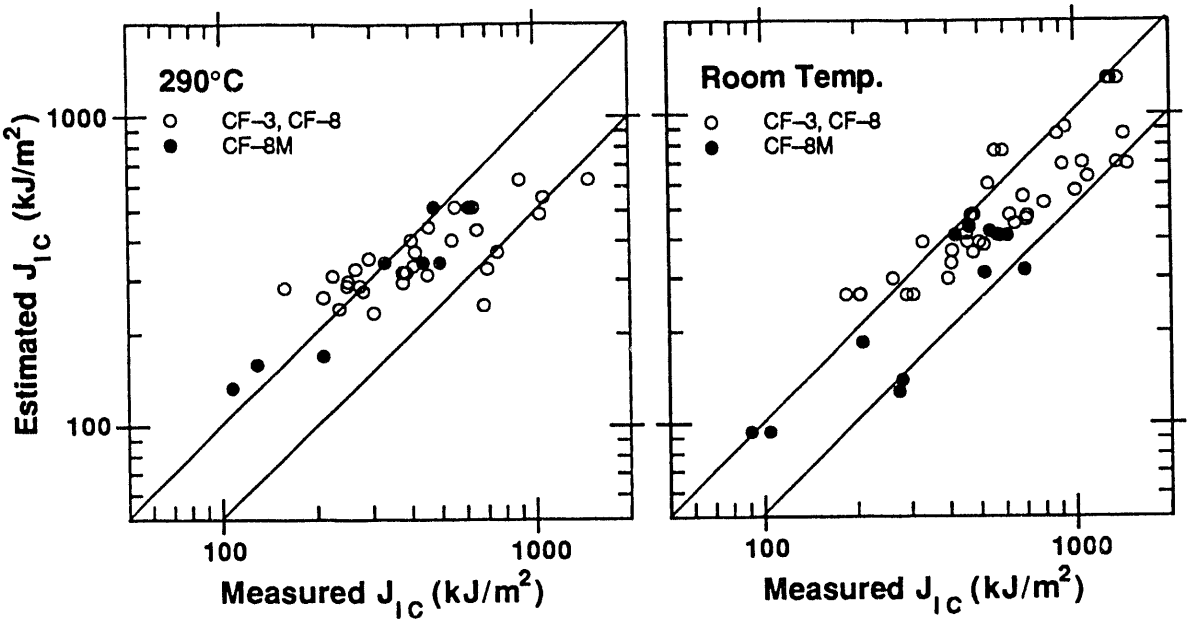

Figure 16. Experimental and estimated values of J_{IC} for aged cast stainless steels at 290°C and room temperature

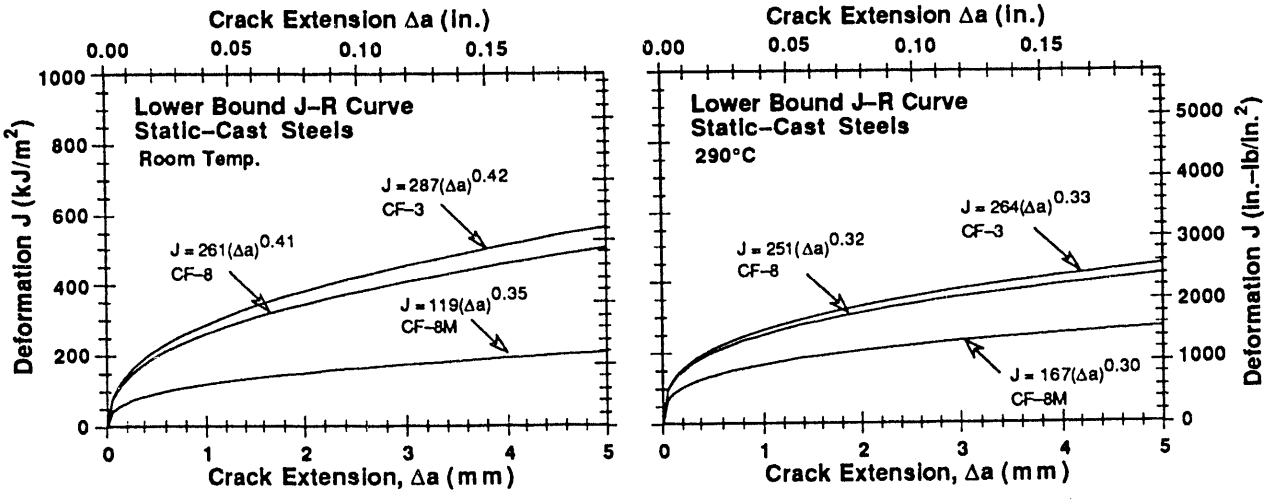

Figure 17. Lower bound J–R curve for static–cast stainless steels at room temperature and 290°C

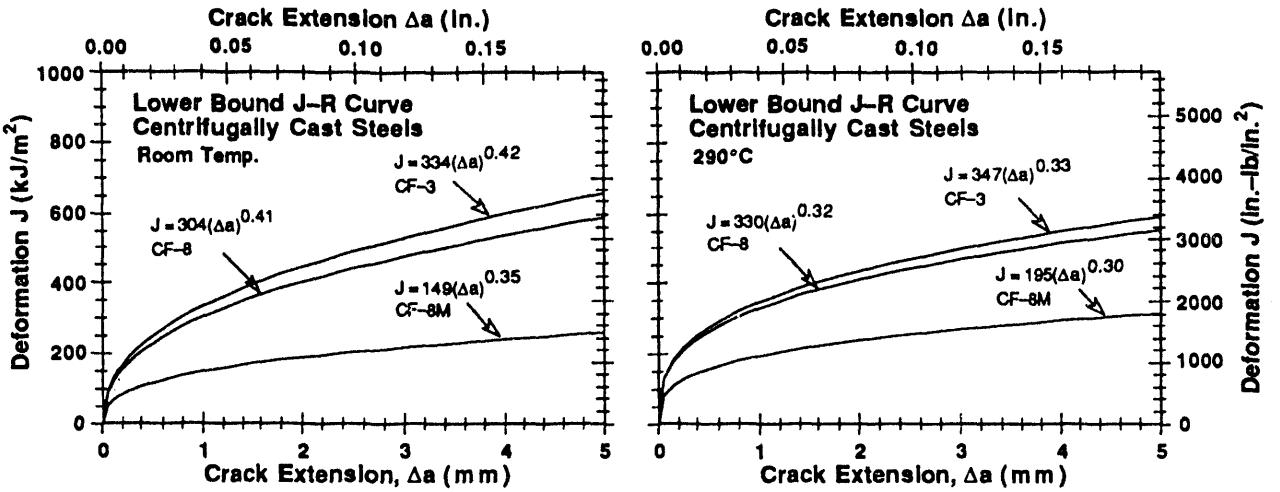

Figure 18. Lower bound J–R curve for centrifugally cast stainless steels at room temperature and 290°C

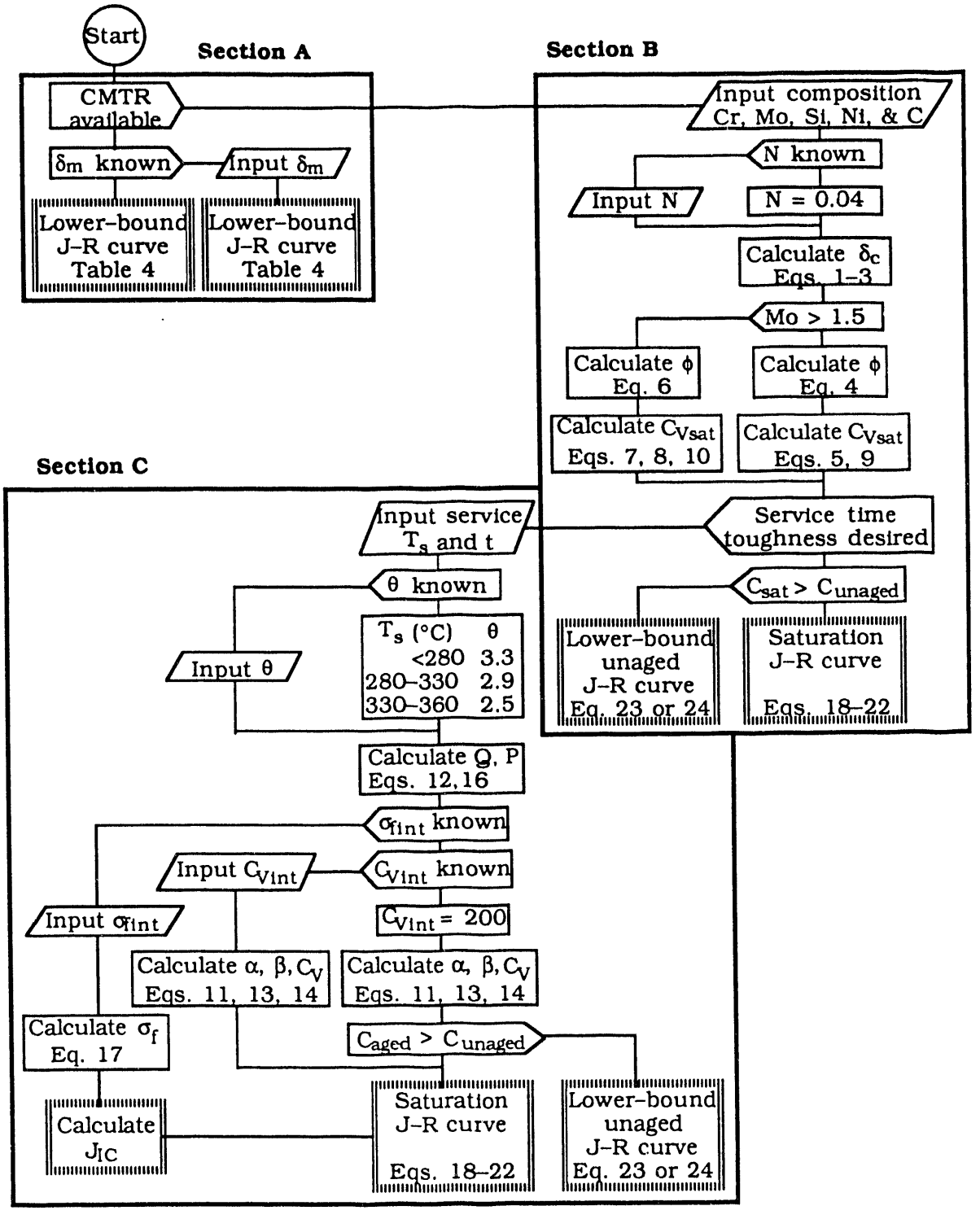

Figure 19. Flow diagram for estimating mechanical properties of aged cast stainless steels in LWR systems

DATE FILMED

4/21/94

END